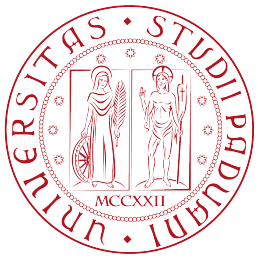

UNIVERSITÀ DEGLI STUDI DI PADOVA

Dipartimento di Fisica e Astronomia “Galileo Galilei”

Master Degree in Astrophysics and Cosmology

Final Dissertation

Intermediate-mass black hole formation in dense massive star clusters

Thesis supervisor

Prof. Michela Mapelli

Thesis co-supervisor

Dr. Sara Rastello

Candidate

Benedetta Mestichelli

Academic Year 2021/22

Abstract

Globular clusters (GCs) are dense ($\rho > 10^3 M_\odot\,\mathrm{pc}^{-3}$), massive ($10^4 - 10^6 M_\odot$) collisional systems often thought to harbor an intermediate-mass black hole (IMBH) at their center. Dynamics plays an important role in such systems, where the most massive objects, including black holes (BHs), tend to segregate in the central regions. Here, the probability of two- and three-body encounters is high, and repeated exchanges and binary hardening can lead to a conspicuous number of binary BH (BBH) mergers.

In this work, we explore the formation channels and properties of IMBHs in young GCs, by means of ninety direct N-body simulations, with masses between 5×10^5 and $10^6 M_\odot$ and metallicity $Z = 0.0002$. We have run the simulations with the new tree-direct N-body code `PeTar` [1], interfaced with our population-synthesis code `MOBSE` [2]. `PeTar` represents a change of paradigm with respect to the past, because it has been designed to simulate star clusters with $\approx 10^6 - 10^7$ stars, which were too massive for previous codes.

We find that six IMBHs form as a consequence of stellar mergers between the components of primordial binaries, while only one of them is the result of a BBH merger. All of the IMBHs have masses of the order of $10^2 M_\odot$, with the heaviest one having $M \sim 229\,M_\odot$. None of them is ejected from the host GC during the time of the simulation, and in two cases the clusters were found to host two IMBHs. From our results, it appears that in such young, massive star clusters the role of dynamics in the formation of IMBHs is reduced, and instead binary evolution gains importance.

We also conducted a study of the main properties of BHs and BBHs. We found that the mass of the binary components of BBHs are preferentially $\leqslant 40 M_\odot$ and that the most massive mergers are related to the evolution of primordial binaries. In addition, the number of merging BBHs increases with the mass of the host GC. It is interesting to notice that the simulated clusters retain $\sim 90\%$ of their BHs, which tend to migrate to the center of the GCs, leading to the formation of possible future BH sub-clusters.

Contents

Chapter 1

Introduction

The possibility of the existence of a central IMBH in GCs has been widely discussed in recent years. IMBHs are compact objects with a mass intermediate between those of stellar-mass BHs ($M \sim 5-10^2 M_\odot$) and those of massive BHs ($M \sim 10^2 - 10^5 M_\odot$); one of their discussed formation channels requires the environmental conditions found in dense, massive star clusters, such as GCs.
The advent of the Hubble Space Telescope (HST) and of integral-field spectrographs on the ground, made it possible to probe the central regions of GCs in search of kinematic signatures of the IMBH presence. Some star clusters (e.g. G1, M15, ω Centauri) were proposed as candidate hosts of IMBHs with masses of the order of $10^4 M_\odot$ ([3],[4],[5]) but no observational proof was as compelling as the one offered by GW190521 [6]. This gravitational signal was detected during the third observational run of the LIGO–Virgo Collaboration, and corresponded to a BBH merger leaving behind a remnant with a mass of $\sim 142 M_\odot$. The future inauguration of gravitational wave (GW) interferometers, such as LISA and the Einstein Telescope, working in a frequency band sensitive to the IMBH mass range [7], is undoubtedly promising for a better understanding of the properties and formation channels of IMBHs.
The scenario according to which IMBHs form in dense stellar systems has also been explored computationally, via direct N-body ([8],[9]) and Monte Carlo simulations ([10],[11]). Because of the enormous computational cost of the direct integration methods, simulations of GCs with $m_{CL} \sim 10^5 - 10^6 M_\odot$ have only been conducted using the latter technique. The advent of performing N-body codes, such as `PeTar` [1], make it possible to simulate massive star clusters with a competitive computational cost, providing at the same time an unparalleled level of precision.
In the current work, we have performed the analysis of ninety simulations generated with `PeTar`, with a mass ranging from 5×10^5 to $10^6 M_\odot$, and an integrated time going from 30 to 100 Myr. Thanks to the tools provided, it was possible to study the evolution of the most interesting objects as single stars or in multiple systems, as well as their probability to be ejected from the cluster. We were also able to analyse the global properties of the GCs, such

as their Lagrangian radii and core densities.
An extensive study of GCs simulations can prove essential to better understand their dynamical history and how the formation of a central IMBH (or BH subcluster) can influence it. A better insight of the present dynamical properties of GCs can help tracing the presence of IMBHs observationally. Moreover, by better constraining the conditions under which IMBHs form in dense, massive clusters, and their main properties (in particular their mass), it is possible to provide a better modeling of the detected GW signals. As a matter of fact, obtaining the merger rates of BBHs leading to the creation of IMBHs (such as GW190521 [12]) and of IMBH binaries (or IMBH-BH binaries) hosted by GCs, helps reducing the parameter space and to model the gravitational signals.

The work is structured as follows: in Chap. 2 we describe the main characteristics of massive dense star clusters, and the formation channels of the BBHs they host, together with a summary of the computational methods used to analyse them; in Chap. 3 we examine the main formation channels of IMBHs, the detection methods and the observational proofs found so far. Chap. 4 reports the computational methods used in this work and the initial conditions of the simulations, as well as the codes used to analyse the output files. Finally, Chap. 5 summarises the main results, focusing on the formation of IMBHs and on the properties of merging BBHs.

Chapter 2

Massive dense star clusters

Star clusters are self-gravitating systems of stars. They form from the collapse and fragmentation of giant molecular clouds and host from a few hundreds to several millions of stars [13]. Initially, such systems are found embedded in their parental molecular cloud, and as a consequence they can be solely observed in the infrared wavelengths. Star formation leads to the disruption of this gaseous cloud, and to the consequent exposure of the cluster.
Star clusters can be classified depending on their age and mass, as well as on their location inside galaxies:

1. **Globular clusters** (GCs) are typically old ($m_{CL} \sim 10 - 12$ Gyr) and very massive, with a mass of $10^4 - 10^6 M_\odot$ [14]. The stars in these systems are tightly bound by gravity, which gives them a typical spherical shape (Fig.2.1). They usually host little to no dark matter, with a mass-luminosity ratio $M/L \sim 2$. They may harbor an IMBH at their center or, as an alternative, a sub-cluster of compact objects. In the Galaxy, such objects can be found mostly in the bulge and in the halo.
   The metallicity of these systems is usually very low, even though galactic GCs have been found to host stellar populations with different contents of C,N,O and Na. The origin of these multiple stellar populations is probably related to a difference in age between the first metal-poor generation of stars and the second one, which forms from a mixture of the pristine gas with the heavier elements generated by the older stars. If evaporated from their host cluster, this first generation of stars must have contributed significantly to the re-ionization of the Universe.

2. **Young massive clusters** are young ($\sim 10^2$ Myr) and can be relatively massive ($m_{CL} \sim 10^2 - 10^5 M_\odot$) (Fig.2.2). They can be referred to as "young globular clusters", as their masses and projected lifetimes correspond to those of GCs [15]. Young, massive star clusters in the Magellanic Clouds span a broad range of ages; on the other hand, their mass and core density are orders of magnitude higher than those of galactic open clusters. Such systems can be found both in the central regions of

the Galaxy and in its spiral arms. Currently, the most massive young cluster known in the Milky Way is Westerlund 1.

3. **Open clusters** are less massive ($m_{CL} \sim 10 - 10^4 M_\odot$), with an age of $\sim$1 Gyr [14]. These systems can be found mainly in the galactic disk. They are usually more metal-rich than GCs, and dominated by massive O and B stars. It has been observed that open clusters in the Galaxy share a number of properties with young and intermediate-age GCs in the Magellanic Clouds, which show no chemical differences between their stellar populations, whose existence is related instead to different rotation rates. Open clusters are mainly found in the vicinity of the galactic plane.

4. **Nuclear star clusters** are extremely massive systems found at the centre of galaxies, which may coexist with a super-massive BHs [16]. They usually have a mass between 10^4 and $10^8 M_\odot$ and are relatively young ($\sim$1 Gyr old).

Figure 2.1: The GC ω Centauri as observed by the WFI camera of ESO's La Silla Observatory. The image is obtained from the composition of the B, V and I filters.

Figure 2.2: Image of the YSC Westerlund 2 and of its surroundings taken by the HST. The central region of the image, containing the star cluster, blends visible light data taken by the Advanced Camera for Surveys and near-infrared exposures taken by the Wide Field Camera 3.
Credits: NASA, ESA, the Hubble Heritage Team (STScI/AURA), A. Nota (ESA/STScI), and the Westerlund 2 Science Team.

2.1 Luminosity profile and initial mass function

When describing the luminosity profile of a star cluster, the King profile [17] is usually assumed

$$f = k\left\{\frac{1}{[1+(r/r_c)^2]^{1/2}} - \frac{1}{[1+(r_t/r_c)^2]^{1/2}}\right\}^2 \tag{2.1}$$

where f is the surface density, r_c is the core radius and r_t the tidal radius (Chap.2.2); an important quantity on this matter is the concentration $c = \log\left(\frac{r_t}{r_c}\right)$. A collection of King profiles can be seen in Fig.2.3. The dynamical King models [18] are instead parametrized by the quantity W_0, which represents the dimensionless depth of the cluster potential well. The empirical and dynamical models are in good agreement for $W_0 \lesssim 7$ ($c \lesssim 0.8$).

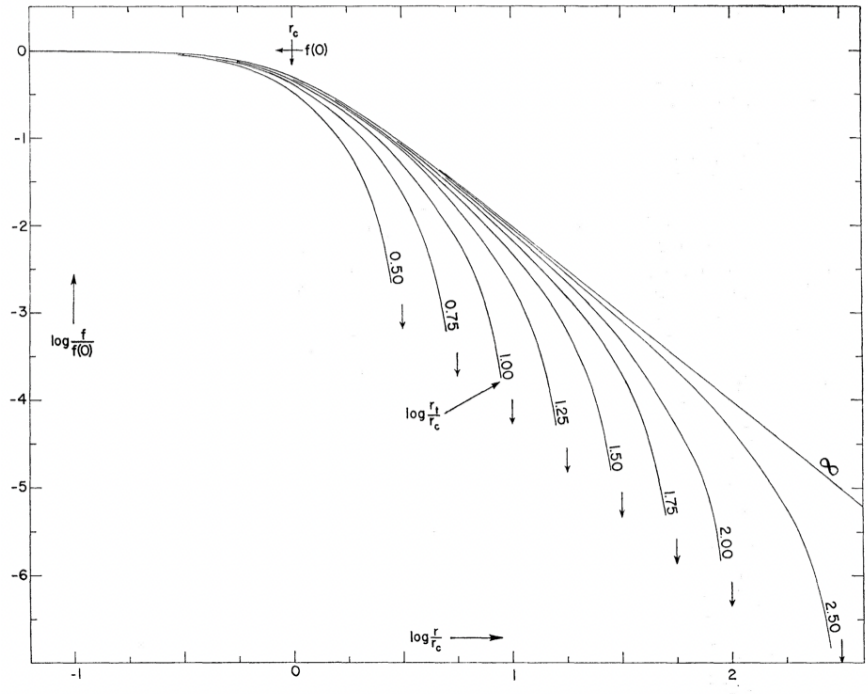

Figure 2.3: Luminosity profiles obtained from Eq.2.1; r_c is the core radius and f_0 is the central surface density [17]

The initial mass function (IMF) is an empirical function describing the initial distribution of masses for a stellar population. The observed stellar luminosities are transformed into estimates of the stellar masses, depending on their evolutionary state. The retrieved mass function is the so-called present-day mass function, which should be corrected for the loss of higher mass stars

due to stellar evolution in order to retrieve the IMF.
According to the first formulation of the IMF from Salpeter [19], the number density of stars with mass in the interval $[M, M + dM]$ is

$$\frac{dn}{dM} \propto M^{-2.35} \tag{2.2}$$

More recently, Kroupa [20] formulated a new relation between the number density of stars and their mass, which depends on the initial mass of the stars themselves and agrees with the relation from Salpeter in the highest range of masses (Fig.2.4)

$$\frac{dn}{dM} \propto \begin{cases} M^{-2.3} & M \geqslant 0.5 M_{\odot} \\ M^{-1.3} & 0.08 \leqslant M < 0.5 M_{\odot} \\ M^{-0.3} & M < 0.08 M_{\odot} \end{cases} \tag{2.3}$$

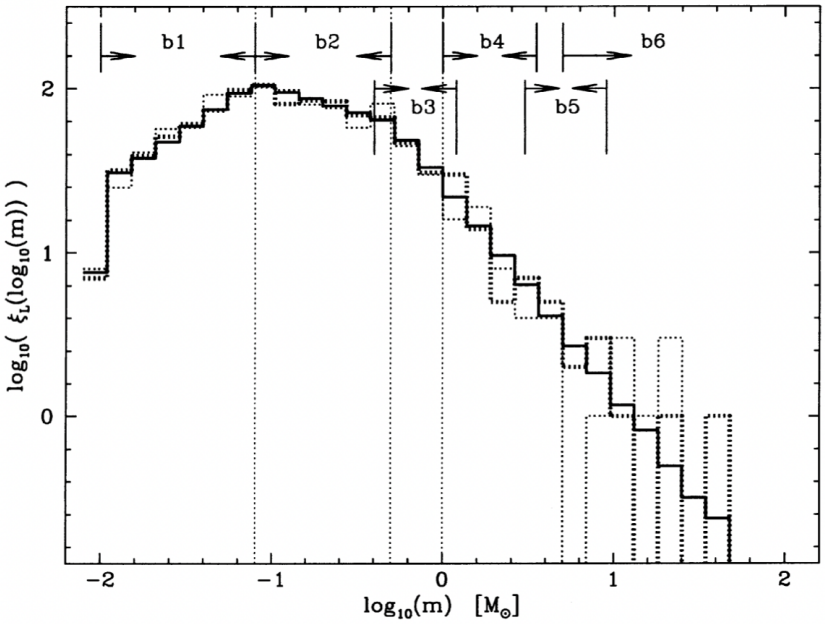

Figure 2.4: Logarithmic rendering of the IMF postulated by Kroupa [20]; $\xi_L(m) = \xi(m) \ln(10m)$, where $\xi(m)$ is the number density of stars in the range of masses [m,m+dm].

The IMF of a cluster changes as a consequence of its dynamical evolution, and therefore it is difficult to link the present-day mass function to the initial one. Moreover, the IMF depends on the binary fraction in the cluster and on the mass-ratio distribution of the binaries.

2.2 Dynamical processes in star clusters

Some operational definitions for star clusters are related to the quantity of mass (or luminosity) contained at a certain distance from the center. The

core radius is the distance at which the surface luminosity of the cluster drops by a factor of 2; the **half-mass (half-luminosity) radius** is the radius within which half of the mass (luminosity) is included. Finally, the **tidal radius** is the distance from the centre at which the gravitational influence of the galaxy on the cluster stars is larger than the influence of the cluster itself.

Star clusters are **collisional systems**, i.e. systems for which the **two-body relaxation time** is small with respect to the Hubble time. The relaxation time is the time needed for a body to completely lose memory of its initial velocity because of two-body encounters with other particles. There are various definitions of this quantity; the simplest definition assumes a spherical system, no rotation and the same velocity v for all stars:

$$t_{rlx} = \frac{N}{8 \ln N} \frac{R}{v} \tag{2.4}$$

with N the total number of stars and R the tidal radius. A more operative definition was given by Binney and Tremaine in [21]

$$t_{rlx} \sim 15 \Big(\frac{M_{TOT}}{10^4 M_\odot} \Big)^{1/2} \Big(\frac{R}{1\text{pc}} \Big)^{3/2} \Big(\frac{1 M_\odot}{m_*} \Big) \text{Myr} \tag{2.5}$$

where M_{TOT} is the total mass of the cluster and m_* is the average mass of stars. On average, GCs are associated to longer relaxation times ($\sim$1 Gyr) with respect to open clusters; a partial overlap is found instead with young star clusters which, as already mentioned, can be very massive. The least massive young clusters can have relaxation times of the order of a few million years, meaning that most of the interactions inside them involve massive stars. GCs instead, having longer relaxation times, are related to interactions between solar mass stars or compact remnants.
The dynamical timescale is related to the time needed by a star to cross the system; the **crossing time** can conveniently be defined as:

$$t_{cross} = \frac{G M^{\frac{5}{2}}}{(-4E)^{\frac{3}{2}}}$$

Because of their collisional nature, GCs are strongly affected by dynamical processes. An example is **mass segregation**, which leads to the migration of stars more massive than the average to the central region of the cluster. If stars with mass m larger than the average mass $\langle m \rangle$ tend to be more centrally concentrated, and if the cluster is much younger than its dynamical friction timescale for stars of mass m ($\sim \langle m \rangle t_{rh}/m$[1]), then the mass segregation is

[1]The half-mass relaxation time t_{rh} is defined by Spitzer [22] as

$$t_{rh} = \Big(\frac{R_c^3}{G M_c} \Big)^{1/2} \frac{N_c}{8 \ln \Lambda_c}$$

considered to be primordial. This means that stars with a mass larger than $\langle m \rangle$ formed preferentially closer to the center. If clusters were the result of the merger of sub-clumps, we would expect the degree of mass segregation of the merger product to be higher [15].
Two-body encounters produce local fluctuations in the energy balance of the cluster, leading to a local change in the velocity distribution of stars. A direct consequence of this are **evaporation** and **core collapse**. As already known, an isolated self-gravitating system must reach virial equilibrium; according to the virial theorem $2K = |W|$ with $K = \sum_{i=1}^{N} \frac{1}{2} m_i v_i^2$ the kinetic energy and $W = -G \sum_{i=1}^{N} \sum_{j>i} \frac{m_i m_j}{|r_i - r_j|}$ the potential energy of the system. From this theorem it follows that stars with a velocity higher than two times the root mean square velocity will evaporate from the system. As a matter of fact, the relaxation time is the time scale on which stars start to follow a Maxwellian distribution; stars found in the tail of such a distribution have velocities larger than the escape velocity and are able to leave the system. Two-body encounters facilitate this process.
Because of evaporation, a stellar system can no longer be considered isolated, and the virial equilibrium is broken. Since the fastest stars are lost, the kinetic energy decreases more strongly than the potential energy and the core contracts; this triggers a runaway mechanism, since the contraction leads to the further loss of fast stars, and to the ulterior collapse of the core. In other words, a self-gravitating system has negative specific heat, so that a reduction of its energy causes the system to heat up. As a consequence, as relaxation transports energy from the warmer core to the cooler outer regions, the central region contracts and warms up [15]. In order to avoid an infinite density at the center of the cluster, a new source of kinetic energy is needed, which is provided by binary-single and binary-binary encounters.
In a star cluster with masses distributed according to an IMF, core collapse occurs at about $t_{cc} \simeq 0.20 t_{rlx}$ [23].

Binary stars can either be **hard** or **soft**. Hard binaries have a binding energy higher than the average kinetic energy of a star in the cluster

$$\frac{G m_1 m_2}{2a} > \frac{1}{2} \langle m \rangle \sigma^2$$

The opposite condition is valid for soft binaries. According to Heggie's law [24] hard binaries tend to become harder (their binding energy increases) while soft binaries tend to become softer as a consequence of three-body encounters.

Three-body encounters can be put in two different categories: **flybys** and **exchanges**. As a consequence of a flyby, the single star can either extract or provide kinetic energy to the binary. In the first case the binding energy

with M_c the total mass of the cluster, R_c the characteristic (half-mass) radius of the cluster and $\ln \Lambda_c \simeq \ln 0.1 N_c \sim 10$ the Coulomb logarithm.

of the binary will increase and the kinetic energy of both the single star and the centre of mass of the binary will increase. In the latter case instead, the binding energy will decrease and the binary could potentially be ionized, i.e. unbound. On the other hand, exchanges are favored when the mass of the single star is larger than the mass of one of the components of the binary and, as a consequence, it is always related to an increase of its binding energy.

2.3 BBH formation in star clusters

Many evolutionary processes can affect a binary of massive stars and its probability to turn into a BBH [21].
In particular, when the binary system is found in a massive dense star cluster, dynamical factors should be taken into account when discussing its evolution. In the central regions of star clusters, where the density is usually higher than 10^3 stars$\cdot$pc^{-3} and the velocity dispersion is of the order of a few tens of kms^{-1}, the two-body relaxation time is shorter than the lifetime of stars. This means that the orbits of single and binary stars are constantly perturbed by dynamical encounters with other members of the cluster.

Mergers of massive stars are common in the cores of young massive star clusters. Under some assumptions, these mergers can lead to the formation of BHs with mass in the pair-instability mass gap ($m_{BH} > 60M_{\odot}$); such massive BHs may acquire a companion by dynamical encounters, consequently leading to a BBH in the mass gap.
A rapid sequence of stellar mergers in the dense cores of young star clusters (**runaway collisions**) might even lead to the formation of an IMBH, especially at low metallicities. Dynamically formed BBHs usually have higher masses than isolated BBHs [25]; in addition, dynamical encounters tend to randomize the spin direction, leading to an isotropic distribution of BH spins. In contrast, isolated BBHs have a preference for aligned spins ([26],[27]).

As already discussed in Chapter 2.2, exchanges are favored when the mass of the perturbing star is larger than the mass of one of the binary components, which is often the case when the perturbing object is a BH. Binaries formed through exchanges have characteristic signatures: they tend to be more massive than average, have high initial orbital eccentricities and their spins are usually misaligned. Dynamical hardening can lead to a speed-up of the merger, by reducing the semi-major axis of the BBH; on the other hand, the least massive BBHs can even be split by three-body encounters with massive intruders.

Massive BHs may also form as a consequence of repeated mergers of stellar-origin BHs that build up to form larger objects (**hierarchical mergers**) [28]. The main obstacle to the formation of second-generation BHs via this channel is the high relativistic kick that the merger remnant receives at its birth; as

a matter of fact, together with energy and angular momentum, GWs carry linear momentum away from a radiating source. Because of the global conservation of linear momentum, the center of mass of the system recoils. The magnitude of the kick depends on the total mass of the system, on the mass ratio q ($= m_2/m_1$) and on the configuration of the BH spins with respect to the orbital plan ([29],[30],[31]). The intensity of the relativistic kick can reach several thousands km s^{-1} and, as a consequence, the BH can easily escape the star cluster; due to their high escape velocities ($v_{esc} \sim 100$km s^{-1}) nuclear star clusters are the most likely to retain the result of hierarchical mergers.
As discussed in [32], if all BHs created from stellar collapse have no spin, more than 10% of BBH mergers from GCs should have at least one component deriving from a previous merger. About 7% of these BBHs should have one component with mass larger than $\sim 55 M_{\odot}$, placing it in the pair-instability supernova mass gap between 60 and 120 $M_{\odot}$, where no compact remnant is expected to be found [33]. Such percentages are increasingly smaller as the spins of the first-generation BHs become larger. Hierachical mergers are one of the most likely formation channels for GW190521 (Chap. 3.2, [12]).

2.4 Computational methods

The two main computational methods adopted for the analysis of collisional systems, and in particular GCs, are N-body codes and Monte Carlo codes.
Direct N-body simulations guarantee an high degree of precision, by directly integrating the set of masses, at the expense of a longer computational time. Monte Carlo methods, instead, are usually less precise but more effective in retrieving the global properties of the clusters. `MOCCA` ([11],[34]) and `CMC` [10] are currently the best alternatives to a direct N-body code, by including N-body models and synthetic binary stellar evolution.

2.4.1 Direct N-body methods

Historically, the first approach to the study of the dynamics of collisional star systems has been a direct summation approach. A direct N-body code computes the gravitational force of every particle on every other particle before summing the individual forces to obtain the instantaneous acceleration of every particle. The gravitational N-body problem can be solved analytically only for $N < 3$, while for $N \geqslant 3$ a solution can be retrieved only numerically.
More specifically, the equation that needs to be solved (for the i-th particle) is

$$\frac{d^2\vec{x}}{dt^2} = -G \sum_{j=1, j\neq i}^{N} m_j \frac{\vec{x_i} - \vec{x_j}}{|\vec{x_i} - \vec{x_j}|^3} \tag{2.6}$$

which can be written as a set of two first-order differential equations

$$\begin{cases} \frac{d\vec{v_i}}{dt} = -G\sum_{j=1,j\neq i}^{N} m_j \frac{\vec{x_i}-\vec{x_j}}{|\vec{x_i}-\vec{x_j}|^3} \\ \frac{d\vec{x_i}}{dt} = \vec{v_i} \end{cases}$$

The number of operations per time-step scales like $O(N^2)$, leading to an enormous computational cost as N approaches the values typical for a star cluster.

The most popular scheme is the **fourth-order Hermite** with block time steps, even though some authors have employed a sixth-order Hermite scheme. It is a predictor-corrector scheme, meaning that the positions and velocities of the particles are firstly predicted at a lower level of accuracy, and then corrected to an higher level using the predictions retrieved beforehand. The algorithm can be summarized as follows:

1. Predictor step:

$$\begin{cases} \vec{x}_{P,i}(t+h) = \vec{x_i}(t) + h\vec{v_i}(t) + \frac{h^2}{2}\vec{a_i}(t) + \frac{h^3}{6}\vec{j_i}(t) \\ \vec{v}_{P,i}(t+h) = \vec{v_i}(t) + h\vec{a_i}(t) + \frac{h^2}{2}\vec{j_i}(t) \end{cases}$$

   with $\vec{j_i}$ the first derivative of acceleration, or jerk.

2. Force evaluation:

$$\begin{cases} \vec{a}_{P,i}(t+h) = -G\sum_{j=1,j\neq i}^{N} m_j \frac{\vec{x}_{P,ij}(t+h)}{x_{P,ij}^3} \\ \vec{j}_{P,i}(t+h) = -G\sum_{j=1,j\neq i}^{N} m_j \left[\frac{\vec{v}_{P,ij}}{x_{P,ij}} - 3\frac{(\vec{x}_{P,ij}\cdot\vec{v}_{P,ij})\vec{x}_{P,ij}}{x_{P,ij}^5}\right] \end{cases}$$

3. Corrector step:

$$\begin{cases} \vec{v_i}(t+h) = \vec{v_i}(t) + \frac{h}{2}[\vec{a_i}(t) + \vec{a}_{P,i}(t+h)] + \frac{h^2}{12}[\vec{j_i}(t) - \vec{j}_{P,i}(t+h)] \\ \vec{x_i}(t+h) = \vec{x_i}(t) + \frac{h}{2}[\vec{v_i}(t) + \vec{v_i}(t+h)] + \frac{h^2}{12}[\vec{a_i}(t) - \vec{a}_{P,i}(t+h)] \end{cases}$$

The initial time-step for particle i is calculated as $\Delta t_i = \eta\frac{a_i}{j_i}$ with η=0.01–0.02 being a good choice. All particles with time-step equal to $\min(\Delta t_i)$ are called "active" particles and their positions and velocities are both predicted and corrected; positions and velocities for the other particles are instead only predicted.
Computing t_i individually for each particle is too expensive, and usually a **block time-step** scheme is adopted. Particles are grouped depending on their individual time-step Δt_i with a block time-step $\Delta t_{i,b} = \left(\frac{1}{2}\right)^n$ where n is chosen according to $\left(\frac{1}{2}\right)^n \leqslant \Delta t_i < \left(\frac{1}{2}\right)^{n-1}$.

Despite their wide use, Hermite integrators are not symplectic in nature.

Symplectic algorithms exactly conserve the surrogate Hamiltonian $\tilde{H}$ ($H = \tilde{H} + H_{err}$). They are built using Hamiltonian splitting: in general, a Hamiltonian is separable if it can be expressed as a sum of two terms H_A and H_B, in which H_A depends only on the canonical coordinates and H_B on the corresponding momenta of the particles. For separable Hamiltonians it is possible to construct first and second-order symplectic integrators, the Euler integrator and the leapfrog integrator.

The **leapfrog method** is a second-order scheme, whose most common version is the KDK (Kick-Drift-Kick). The algorithm can be summarized as follows:

$$\begin{cases} \vec{x_i}(t+h) = \vec{x_i}(t) + h\vec{v_i}(t) + \frac{h^2}{2}\vec{a_i}(t) \\ \vec{a_i}(t+h) = -G\sum_{j=1,j\neq i}^{N} m_j \frac{\vec{x_i}(t+h)-\vec{x_j}(t+h)}{|\vec{x_i}(t+h)-\vec{x_j}(t+h)|^3} \\ \vec{v_i}(t+h) = \vec{x_i}(t) + \frac{h}{2}[\vec{a_i}(t) + \vec{a_i}(t+h)] \end{cases}$$

An alternative version is the DKD (Drift-Kick-Drift), in which positions are evaluated at the midpoint instead of velocities.

When $x_{ij} = |\vec{x_i} - \vec{x_j}| \to 0$ the so-called *ultraviolet divergence* is found; it corresponds to a singularity in the gravitational potential, which is achieved for very close encounters. This problem can be solved numerically using two different methods: softening and regularization.
In fact, the UV divergence can be solved by introducing a softening parameter ϵ in the interaction potential $\left(U_{ij} = \frac{Gm_im_j}{\sqrt{x_{ij}^2+\epsilon^2}}\right)$, but this solution introduces a loss of resolution of the order of ϵ and below.
On the other hand, **regularization** removes the singularity in the potential by performing a change of coordinates. One of the most used regularization techniques in direct N-body codes is the Kustaanheimo-Stiefel (KS) regularization [35]. It is an extension of Levi-Civita's regularization of the planar Keplerian problem to three dimensions. The Keplerian orbit is transformed into an harmonic oscillator, reducing the integration steps significantly; the centre-of-mass and relative motion of binary systems are integrated separately. On the other side, in the case of perturbed two-body motions, KS already proves inefficient. The treatment of multiple ($N \geqslant 3$) encounters is simplified by the concept of chain regularization; the basic idea is to connect the main two-body interactions with a chain of KS-type variables which is updated anytime the non-chained terms become large (Aarseth and Mikkola [36]).

The enormous computational cost of a direct integration of massive star clusters, such as GCs, has lead in the 1980s to the construction of a special-purpose computer, GRAvityPipE (GRAPE, [37]) by Sugimoto, Hut and Makino. GRAPE is a hardware implementation of Newtonian pair-wise force calculations between particles in a self-gravitating N-body system; the latest version (GRAPE-6) was released in 2001. At the beginning of the millennium, Graphics Pro-

cessing Units (GPUs) began replacing Central Processing Units (CPUs) and GRAPE boards in the implementation of direct summation algorithms. The initial purpose of GPUs was to manage graphics with an high level of data parallelism; this is the concept behind the SIMD/SIMT (Single Instruction Multiple Data/Threads) technique. A new GPU concept was born mostly thanks to CUDA (Compute Unified Device Architecture), which was developed by Nvidia in 2006 and can be considered an extension of high-level programming languages such as C,C++ and Fortran to the GPU architecture.

The first implementation of a fourth-order Hermite scheme with block time-steps using GPUs was performed by Portegies Zwart et al. in 2007 [38]. The N-body code was written in Cg (C for graphics). They found that the GRAPE-6Af workstation outperformed the GPUs for $N \lessapprox 10^4$ particles, mainly because of an inefficient memory access and additional overhead cost. In addition, the energy error produced using GRAPE was one order of magnitude smaller than the one obtained using GPUs.
Capuzzo-Dolcetta et al. developed a code (`HiGPU`) able to couple the computing power of GPUs to the precision guaranteed by a sixth-order Hermite scheme with hierarchically blocked time-steps[2][40]. The code was written in C and C++ and parallelized using OpenMP and CUDA; since the evaluation step and the corrector step are the most computationally expensive, they were both implemented on GPUs, while the less demanding one was left to CPUs. The efficiency of the code was shown to scale with the number of integrated particles (up to 8×10^6).
The `NBODY` series [41], and in particular `NBODY6++GPU` [42], contains state-of-the-art algorithmic and hardware optimizations that enable the integration of systems with $N \sim 10^6$ particles, including stellar evolution and primordial binaries. The code makes use of a fourth-order Hermite integration method with hierarchical block time-steps and, in addition, it implements an Ahmad-Cohen neighbor scheme. This scheme relies on the separation of the integration process in two parts: the so-called regular force is the summation of forces from particles outside the neighbor radius, while the irregular force accumulates only the neighbor forces. The positions and velocities calculated during a previous regular step are used for prediction during the next irregular step; the resulting speed-up is proportional to $N^{1/4}$. On the other hand, this gain is reduced in parallel computing because of the difficult implementation of the algorithm. `NBODY6` [41] also makes use of the KS regularization and of the chain regularization to deal with close encounters, binaries and multiple systems. `NBODY6++` [43] is based on `NBODY6`, making use of MPI parallelization with the copy algorithm; each MPI processor integrates different subsets of active particles, while having the complete particle dataset at disposal. Finally, `NBODY6++GPU` implements the OpenMP, CUDA and AVX/SSE parallel

[2] $\Delta t_n = \frac{\Delta t_{max}}{2^{n-1}}$ with n the integration step and Δt_{max} a predefined maximum time-step [39]; at each time-step, active particles are integrated together.

methods to make the code as fast as possible.
The N-body code used to produce the simulations which will be later analysed in this work is `PeTar` [1], whose characteristics are widely discussed in Chap.4.2.

2.4.2 Monte Carlo methods

The alternative approach to direct summation is the orbit-averaged Monte Carlo method, originally developed by Hénon in 1971 [44]. Since the number of particles in a star cluster is very high, the gravitational field can be modelled as the sum of a main mean field and a small irregular field. The time-step Δt is chosen to be much larger than the crossing time but much smaller than the relaxation time; in such time interval, the effect of the fluctuating field on stars can be neglected in a first approximation. As a consequence, the orbital motion of the star will be described by a simple analytical expression. Over a time of the order of t_{rel}, the effect of the irregular field will build up; in order to account for it, instead of integrating the interaction with every other particle in the system, a Monte Carlo approach is employed. The perturbation is computed only in one point along the orbit, and the effect of one star (chosen among all the field stars) is taken into account. Thanks to these considerations, the computational time is proportional to N, against the $O(N^3)$ of the direct N-body codes.

The two main codes based on the Hénon N-body method are the Cluster Monte Carlo (`CMC`, [10]) and the Monte Carlo Cluster Simulator (`MOCCA`, [11]).
`CMC` is a parallel code able to describe the evolution of massive, spherical star clusters, such as GCs; it contains the treatment of two- and three-boy binary formation, strong encounters between single stars and binaries (thanks to a small-N direct integrator, `FEWBODY` [45]), galactic tidal fields, physical collisions and post-Newtonian dynamics. It also contains single and binary stellar evolution, using the `COSMIC` population synthesis code (based on `BSE` [46]).
`MOCCA` is a numerical code able to simulate real star clusters with a degree of accuracy comparable to that of direct N-body codes, but significantly faster (a few days for a GC). It incorporates a treatment of all the relevant physical processes in the evolution of a star cluster, such as multiple interactions (using `FEWBODY`), relaxation, stellar evolution of binary and single stars with `BSE` [46], escapers and binary formation from three-body interactions. This last aspect is not treated using `FEWBODY`, but instead the probability to form a binary star from the encounter of three single stars depends only on the local number density of stars.

Chapter 3

Intermediate-mass black holes

IMBHs are BHs with a mass intermediate between the one of stellar mass BHs ($\sim 5 - 10^2 M_\odot$) and the one of massive BHs (larger than $10^4 M_\odot$).

3.1 Formation channels

The formation channels of IMBHs are various and correspond to different mass ranges and environmental conditions.
In the first scenario, IMBHs form from the direct collapse of dense gas clouds at high redshifts ($z \sim 10 - 20$); in this case they can reach masses of the order of $\sim 10^4 - 10^6 M_\odot$. The direct collapse paradigm is based on two main conditions: the gas should be atomic to prevent fragmentation and formation of Population III (Pop III) stars and the inflow rate should be kept high. As a consequence, the presence of a strong UV background radiation field is required to guarantee the dissociation of H_2. The main problem of this model is related to the disposal of the residual angular momentum at the collapse; a possible solution can be found in [47] and is related to global dynamical instabilities driven by self-gravity ("bars within bars" mechanism).

A second formation channel hypothesizes instead that IMBHs are the result of the collapse of PopIII stars. These stars have zero metallicity by definition and the final products of their evolution would very likely have a mass larger than 100 $M_\odot$. As a matter of fact, PopIII stars may die losing a very small fraction of their mass – the mass loss by stellar winds depends on the metallicity of the star $\dot{M} \propto Z^\alpha$ – so that a very massive star (VMS) with $100 \leqslant m \leqslant 250 M_\odot$ will either undergo pair-instability and disappear in a nuclear explosion (mass of the He core smaller than 135 $M_\odot$) or collapse directly into a BH [48].

A third family of models assumes that IMBHs are formed in dense stellar systems. This scenario has been explored both analytically [49] and computationally, via direct N-body simulations ([8],[9]) and Monte Carlo simulations (`MOCCA` [11], `CMC` [10]).

Portegies Zwart et al. ([50], [23], [51]) showed that stars with an higher mass preferentially participate to collisional encounters. Young massive star clusters may experience an early evolutionary phase during which the central density is so high that physical collisions between stars become frequent. In [23] the authors retrieve a mass accumulation rate due to collisions $\dot{M} \simeq 10^{-4} m_{CL}/t_{rh}$, with m_{CL} the mass of the cluster and t_{rh} the half-mass relaxation time. The condition for the set-up of this mass accretion is that the initial t_{rh} of the cluster is less than ∼30 Myr, so that the most massive stars, which drive the runaway collisions, are able to segregate to the central region of the system before experiencing supernovae, leading to an early core-collapse. If the cluster is born sufficiently concentrated ($W_0 \gtrapprox 9$) a longer half-mass relaxation (∼100 Myr) can still lead to a runaway mass growth. The final mass of the interested object can reach up to $\sim 0.1\%$ of the initial cluster mass, leaving behind a compact object in the mass range of IMBHs.
Miller and Hamilton proposed a different formation mechanism in [52], according to which a central BH grows significantly by accretion. As a matter of fact, a $\gtrapprox 50 M_\odot$ BH has enough inertia to remain bound to the parental system; it will sink to the centre of the cluster in $\lessapprox 10^6$ yr, where, in the ∼10 Gyr lifetime of the GC, it will accrete up to $\sim 10^3 M_\odot$.
Giersz et al. (`MOCCA` [34]) confirmed the existence of these two main formation channels of IMBHs in dense star clusters. The first one (FAST) is set during the first evolutionary phases of the cluster, after the formation of neutron stars and BHs via supernovae explosions, and the formation of a BH sub-cluster in the system (central density of $\sim 10^8 M_\odot \mathrm{pc}^{-3}$). Alternatively, if all BHs but one are removed from the cluster, the SLOW scenario will take place, involving a lower accretion rate (density $\sim 10^5 M_\odot \mathrm{pc}^{-3}$).
The work by Mapelli [8] analyses young massive star clusters with low metallicity through a direct N-body simulation. It shows that massive objects tend to migrate to the central region of the cluster because of mass segregation; here, they will have an higher probability to experience dynamical encounters and enter binary systems. Massive objects undergoing multiple collisions can evolve in a very massive blue straggler star and then collapse to an IMBH; VMSs could also collapse directly into an IMBH without experiencing runaway collisions.

3.2 Detection methods and observations

If we consider the relation between the mass of a super-massive BH and the velocity dispersion in its host galaxy, it is expected that GCs host BHs with masses between 10^3 and $10^4 M_\odot$. Because of the small amount of gas and dust in a GC, a small accretion rate is foreseen, and for such reason the detection of IMBHs in the X-ray and in the radio frequencies is quite challenging. As a consequence, the observational proof of IMBHs is mainly found by studying the kinematics of the central region of star clusters. Thanks to the observa-

tions made by the HST, and to the advent of integral-field spectrographs on ground, it was finally possible to conduct a search for these objects.

A number of GCs have been proposed to harbor IMBHs at their centers. M15 is a galactic cluster that is assumed to be in a post-core collapse state; it could either contain a BH or a sub-cluster of compact remnants at its center. G1 is instead a giant GC found in M31; the presence of an IMBH here is supported by X-ray and radio observations.

ω Centauri (NGC 5139) is the most massive GC in the Galaxy, with a mass of $2.5 \times 10^6 M_\odot$ and a central velocity dispersion of 22 ± 4 km s^{-1}. Noyola et al. [3] found proof of the presence of an IMBH with a mass of $4 \times 10^4 M_\odot$ in the cluster from both photometry and kinematics. The surface brightness curve was obtained from the image taken by HST and it showed a logarithmic slope of -0.08 ± 0.03 at the center; as a matter of fact, the presence of a BH should prevent the core collapse and leave the imprint of a shallow cusp. The main evidence was provided by the increase of the central velocity dispersion from 18.6 to 23 km s^{-1} from radii 14" to 2.5". These results were questioned by Van der Marel and Anderson [5], who found that the projected density profile was flat with an upper limit of 0.07 for the central logarithmic slope; this would lead to a maximum mass of $1.2 \times 10^4 M_\odot$ for the central IMBH (Fig.3.1).

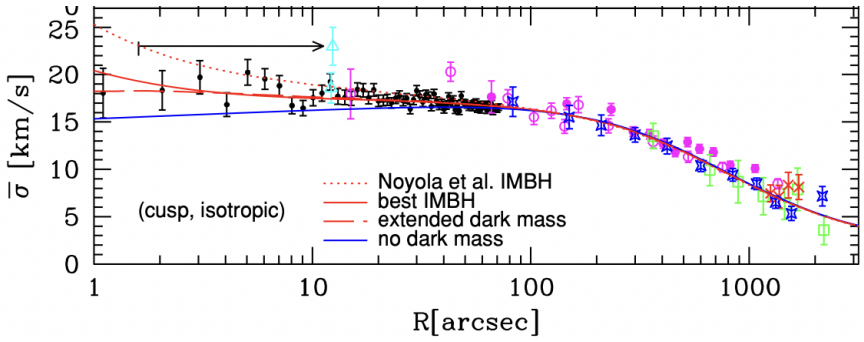

Figure 3.1: Velocity dispersion profile of ω Cen with various central BH models (red dashed line: Noyola et al. [3], red solid line: Van der Marel [5]).

G1 and ω Centauri are atypical clusters, both of them being the most massive GCs in their host galaxies. They are hypothesized to be the nuclei of dwarf galaxies stripped of their outer layers, and as such they should be regarded as nuclear star clusters, with their central BH being the low-mass tail of the distribution of super-massive BHs.

Noyola et al. also discussed the presence of a BH at the center of NGC 6388 [4]. This cluster is located 11.6 kpc away from the Sun, in the outer part of the

Bulge; it has a mass of $\sim 1.3 \times 10^6 M_\odot$ and a central velocity dispersion of 18.9 kms^{-1}. By analysing photometric and spectroscopic data, it was estimated that the central IMBH has a mass of $(1.7 \pm 0.9) \times 10^4 M_\odot$ (Fig.3.2).

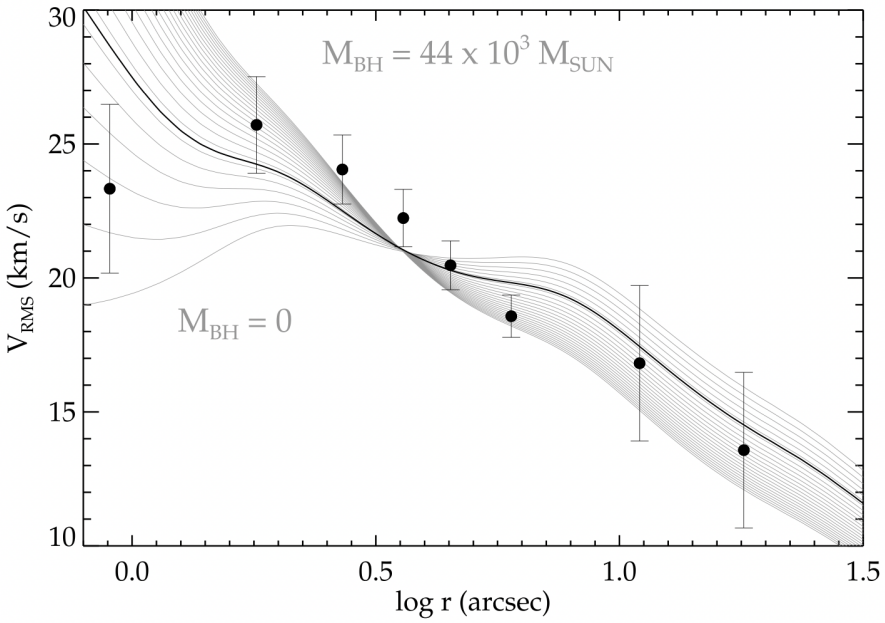

Figure 3.2: Data and models of the velocity dispersion profile of NGC 6388 [4]; the solid grey lines correspond to different masses of the central IMBH (from $M_{BH} = 0$ to $M_{BH} = 4.4 \times 10^4 M_\odot$).

Further observational evidence of the existence of IMBHs was given by the discovery of ultra-luminuous X-ray sources in non-nuclear positions in starbust galaxies. Such sources are believed to be accreting IMBHs with masses larger than $10^3 M_\odot$ (L$\sim 10^{41}\mathrm{ergs}^{-1}$) [53].

The most compelling proof of the existence of IMBHs so far was given by GW190521 [12]. This signal was detected from searches for quasi-circular binary coalescences, and it is consistent with the merger of two BHs with masses of 85^{+21}_{-14} and $66^{+17}_{-18} M_\odot$. A representation of the GW event observed by the LIGO–Virgo Collaboration is shown in Fig.3.3. The mass of the heavier binary component has a high probability to lie within the pair-instability supernova mass gap. The mass of the remnant was calculated to be $142^{+28}_{-16} M_\odot$, making this the first direct detection of an IMBH. Because of the large mass of the binary components, the detected signal had a short duration. In the future it is expected that the sensibility of the LIGO and Virgo detectors will improve at low frequencies, making it possible to detect more of such signals. Moreover, third generation space and ground interferometers such as LISA and the

Einstein Telescope will operate in a frequency interval interested by signals generated by mergers in the mass range of IMBHs [7].

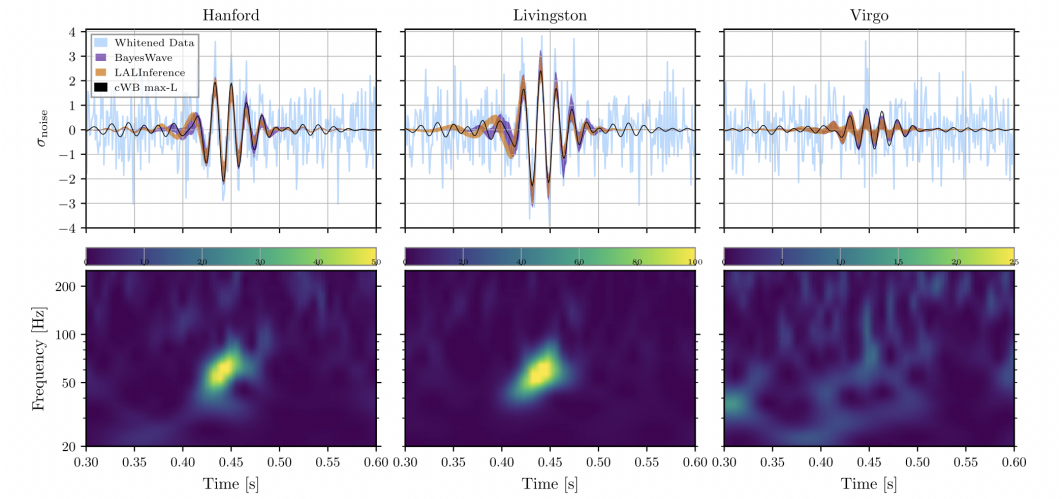

Figure 3.3: The GW event GW190521 as observed by the LIGO Hanford, LIGO Livingston and Virgo detectors. *Top panel*: time-domain detector data after whitening by each instrument's noise amplitude spectral density. *Bottom panel*: time-frequency representation of the whitened data [12].

Chapter 4

Computational methods

In the present discussion, we have made use of `PeTar` [1], a software developed to study collisional systems and follow the dynamical and stellar evolution of single and multiple objects (binaries, triples etc.).

4.1 Initial conditions of the simulations

The initial conditions were generated with `mcluster` [54]. This tool is an open source program that can be used to either set up initial conditions for N-body computations or, alternatively, to generate artificial star clusters directly.

Ninety simulations were generated with an initial mass ranging from 5×10^5 to $10^6 M_\odot$. The clusters were assumed to present no primordial mass segregation. A King profile was chosen as the radial density profile, with an initial half-mass radius r_h=5 pc, and a concentration parameter W_0=5 [18]. The IMF is a broken power-law with a slope $\alpha = -1.3$ between 0.1 and 0.5 $M_\odot$ and $\alpha = -2.3$ for higher masses, with an initial maximum mass of 150 $M_\odot$. All simulations were generated with a primordial binary fraction $b = 0.4$; primordial binaries are binary systems already bound to the cluster at its formation. The chosen metallicity for the simulated clusters corresponds to one hundredth of the solar one ($Z = 0.0002$). The clusters are in presence of a tidal field which can be described using a linearized approximation [55]. The set of initial conditions is reported in Table 4.1.

In order to reproduce the conditions found by Sana et al. [56] and the observational results found by Moe and Di Stefano [57], an ulterior algorithm was implemented [58]. For binary systems, a mass ratio distribution $F(q) \propto q^{-0.1}$ with $q \in [0.1, 1]$ was assumed [56]. The binary fraction for the primary mass in different mass ranges (expressed in $M_\odot$) was set to: $f_{b,[0.1,0.8]} = 0$, $f_{b,[0.8,2]} = 0.4$, $f_{b,[2,5]} = 0.59$, $f_{b,[5,9]} = 0.76$, $f_{b,[9,16]} = 0.84$ and $f_{b,[16,150]} = 0.94$ [57]. Finally, the orbital period and eccentricity distributions were generated following [56]. In particular, the orbital periods were randomly drawn from $F(\mathcal{P}) \propto \mathcal{P}^{-0.55}$

with $\mathcal{P} = \log_{10}(P/\text{days}) \in [0.15, 5.5]$ and the eccentricities from $F(e) \propto e^{-0.45}$ with $e \in [10^{-5}, e_{max}(P)]$. For a given orbital period, an upper limit was set to the eccentricity distribution $e_{max}(P) = 1 - \left[\frac{P}{2\text{ days}}\right]^{-2/3}$.

Initial conditions of the clusters generated with `mcluster`	
Initial mass (M_i)	5×10^5 – $10^6 M_\odot$
Half-mass radius (r_h)	5 pc
Concentration (W_0)	5
Minimum mass (m_{min})	0.1 $M_\odot$
Maximum mass (m_{max})	150 $M_\odot$
Binary fraction (b)	0.4
Metallicity (Z)	0.0002

Table 4.1: Initial conditions of the simulations

4.2 PeTar

`PeTar` combines three integration methods:

1. **Barnes-Hut tree** [59] to calculate long-range forces between particles, which are computed using a second-order symplectic leap-frog algorithm (Chap.2.4.1)

2. **Fourth order Hermite integrator** with block time steps (Chap.2.4.1) to integrate the orbits of stars and the centers of mass of multiple systems

3. **Slow-down algorithmic regularization method (SDAR)** [60] to integrate multiple systems.

Because of its parallel hybrid formalism, `PeTar` is able to run realistic simulations of clusters with up to $\sim 10^7$ bodies in a competitive time. As a matter of fact, the computational cost of this method is $O(N \log N)$, with respect to the usual $O(N^2)$ cost of direct N-body algorithms. As a consequence, the code is able to handle an arbitrary number of multiple systems. In order to obtain a good performance on multiple-core computers, the code is implemented with FDPS [61], which provides an excellent MPI and OpenMP parallelization of the particle-tree (PT) part for the long-range forces calculation. The particle-particle (PP) particle-tree method (P^3T) was firstly introduced by Oshino et al. [62] to simulate collisional systems with a multiple timescale issue, and it was found to be ten times faster than the Hermite method [63]. The neighbour searching and long-range force calculation (P^3T-kick) are optimized by the use of SIMD instructions (AVX, AVX2, AVX-512) and GPU acceleration (CUDA). The SDAR library is used instead to perform the P^3T-drift (short-range interactions); this part is parallelized by using OpenMP in each MPI

processes.

The stellar evolution is handled with the implementation of `MOBSE`/`MOSSE` [2]. It is currently possible to choose among three stellar evolution packages based on `BSE` and `SSE` ([64], [46]).
Moreover, `PeTar` is interfaced with `Galpy` [65], an advanced software used to model the Galactic tidal field.
The main code is written in C++ language, while the data analysis tools are written in Python3.

Once the file with the initial conditions has been generated, reporting the values of the masses, velocities, and positions of the stars, it needs to be modified to be read and used by `PeTar`; in order to do so, the *petar.init* tool is used. Since both the stellar evolution and the presence of a tidal gravitational field have been assumed, extra columns were added to the existing ones.

At this point, it is possible to start the simulations by using the *petar* command so to obtain the output files that will later be analysed. It is possible to specify the number of options when generating the data files. In particular, we specified the model chosen for the formation of neutron stars and BHs as the rapid supernovae model [66], according to which neutron stars with a mass larger than $2M_{\odot}$ shouldn't be produced, as well as BHs with masses lower than $5M_{\odot}$. Most of the BHs should be formed without supernovae explosions and only a small fraction of the low-mass ones would experience a natal kick. The model chosen for the treatment of the BH natal kick was the one provided by Giacobbo and Mapelli in [67], according to which $v_{kick} \propto f m_{ej}^{-1} m_{rem}$, where f is a random number drawn from a Maxwellian distribution with one-dimensional root mean square $\sigma = 265$ kms^{-1}, m_{ej} is the mass of the ejecta and m_{rem} is the mass of the compact remnant. Moreover, the α (energy removal efficiency) and λ (geometrical factor) coefficients for the binding energy of the common envelope were specified as $\alpha = 1$ and $\lambda = 0.1$[1]. Finally, the finishing time and frequency of the outputs can be chosen: for the first 20 Myr, the files were produced every 0.125 Myr, and later only once every million year. An example of a file containing the commands needed to generate the initial conditions of the simulations and initiating them with `PeTar` ("loop" file) is found in Appendix A.2.

Together with the snapshot files produced at each time-step and describing the conditions of the single and multiple objects inside the cluster, the output consists of other types of files reporting information on the status of stellar evolution, the global properties of the cluster and its energetic content. For example, *data.group* contains information about new multiple systems as well

[1] The formulae relating these coefficients to the initial binding energy of the envelope are respectively $E_{bind,i} = \alpha(E_{orb,f} - E_{orb,i})$ and $E_{bind,i} = -\frac{G}{\lambda}\left(\frac{M_1 M_{env,1}}{r_1} + \frac{M_2 M_{env,2}}{r_2}\right)$

as disrupted ones; *data.status* reports the global parameters of the cluster, such as the energies, angular momenta, number of particles and the center position and velocity of the system. When the stellar evolution is also considered, *data.mosse* and *data.mobse* report information on the evolution of single and multiple objects respectively.

The snapshot data files can be processed further to provide information about single, binary and multiple objects specifically; a new set of files with the suffices *.single* and *.binary* (as well as *.triple* etc.) will be produced. Moreover, *petar.data.process* creates files describing Lagrangian and core properties of the cluster (*data.lagr* and *data.core*) and information about single and binary escapers (*data.esc_single* and *data.esc_binary*). The snapshots are shifted to the rest frame where the coordinate origin corresponds to the density center. By adding the core position and velocity from *data.core* at the corresponding time, the positions and velocities in the Galactocentric frame (when `Galpy` is used) can be recovered. The *data.lagr* file includes the radius, average mass, number of objects, velocities and dispersions within different Lagrangian radii. The mass fraction contained in each Lagrangian radius is [0.1, 0.3, 0.5, 0.7, 0.9] by default; the properties at the core radius are added last. When stellar evolution is considered as well, it is possible to compute the Lagrangian properties of specific types of stars as well; this tool is useful to understand whether a sub-cluster of compact objects is present at the center of the system.

If MPI is used, each MPI processor generates individual data files. As a consequence, some output filenames will contain the suffix "MPI rank". The *petar.data.gether* command is used to gather these output files from different MPI ranks to one file. The files related to the dynamical and stellar evolution of the objects of the cluster are especially interesting in the context of this work. The *data.mobse.type_change* file contains information about the stellar type changes experienced by binary systems, such as evolutionary changes, Roche lobe mass transfers, common envelope phases and disruptions. Finally, *data.mobse.dynamic_merge* analyses dynamically driven (hyperbolic) mergers.

4.3 Computer clusters

The simulations were mainly run on the MARCONI100 (M100[2]) cluster at CINECA; this accelerated cluster is based on IBM Power9 architecture and Volta NVIDIA GPUs. It consists of 980 compute nodes and 8 login nodes characterized by the same structure. Each node consists of 2 Power9 sockets, each of them with 16 cores and 2 Volta GPUs (32 cores and 4 GPUs per node). The multi-threading is active as well, with 4 threads per physical core (128 threads – logical CPUs – per node).

[2] `https://www.hpc.cineca.it/hardware/marconi100`

As usual in High-Performance Computing systems, large production runs are executed in batch mode. A "job" file will be written and submitted to the SLURM scheduler, which will look for the resources requested by the user and provide them as soon as they are available. Such file will have to report the maximum duration of the run, the partition (*m100_usr_prod*), and the requested resources. In this specific case, we chose not to make use of the parallelization; one node per time was requested, with 1 MPI process and 64 logical CPUs per node. An example of a job file is reported in Appendix A.1.

Because of the ten-minute CPU-time limit in the interactive environment of M100, the analysis of the output files was mainly carried out locally.

4.4 Codes

In order to read the output files described in the previous section, `PeTar` provides a set of tools written in Python3.
With the aim of analysing the global properties of the cluster, I have written a simple code in Python3 giving back the evolution of the Lagrangian radii of the cluster with time. It is possible either to take into account all the stars in the clusters or only certain stellar types; this tool is particularly useful to keep track of the position of compact objects and understand whether they form a sub-cluster. Thanks to the *petar.LagrangianMultiple()* tool it is also possible to give an estimate of the central density of the cluster and to compute the relaxation time of the GC.

The unprocessed data files were firstly analysed looking for IMBHs; their identification number was retrieved and, consequently, the *data.mobse* files were studied in order to assess whether the IMBH was the result of stellar evolution or hyperbolic merger and to determine the probable supernova kick it received (Appendix A.3). Then, the *.single*, *.binary* and *.triple* data files were analysed to obtain the evolution of the star as a single, in a binary or in a triple system (Appendix A.4). Finally, it was possible to assess if the IMBH was the evolutionary result of one or more collisions between stars, or the result of the merger between previous generations of BHs.

Thanks to the *petar.BSETypChange()* tool it was possible to retrieve the number of merging BBHs in each simulation. The distribution of their primary and secondary mass and their mass ratio were also obtained.

In conclusion, by means of the *petar.SingleEscaper()* and *petar.BinaryEscaper()* tools I obtained the number of BHs (both single and inside a binary) that escaped the clusters and compared it to the total number of BHs.

Chapter 5

Results

In the next chapter, we will explore the results found from the analysis of the simulated GCs. The results concerning IMBHs and their formation channels are reported in Chap.5.2; Chap.5.3 contains an analysis of the main properties of BHs and BBHs, focusing in particular on merging BBHs. In Chap.5.4 we evaluate the possibility of the presence of a BH sub-cluster in young GCs, and finally in Chap.5.5 we show the evolution of the Lagrangian radii of the simulated clusters.

5.1 Initial properties

The initial density distributions of five simulations in the mass range between 5×10^5 and $10^6 M_\odot$ are shown in Fig. 5.1. In Table 5.2 the initial values of the two-point relaxation time and of the central density for the same mass range are also reported. The relaxation time is of the order of some billion years, leading to a core-collapse timescale ($t_{cc} \simeq 0.20 t_{rlx}$, Chap.2.2) of a few hundred million years. Our analysis will follow the evolution of pre-collapsed dense massive star clusters for a duration depending on their mass and reported in Table 5.1.
As a matter of fact, the simulations were run for a total of one month on the M100 cluster at CINECA and the heavier ones required longer integration times. Initially, we expected to run the simulations for at least three months, but during the analysis of the first sets of results, I found a bug related to the `MOBSE` dynamic merger tool, which resulted in the assignment of the wrong stellar type to the product of hyperbolic mergers. This bug was solved and the new version of `PeTar`[1] was used to run the simulations again.

[1]This version can be found in: https://github.com/SaraRastello/PeTar

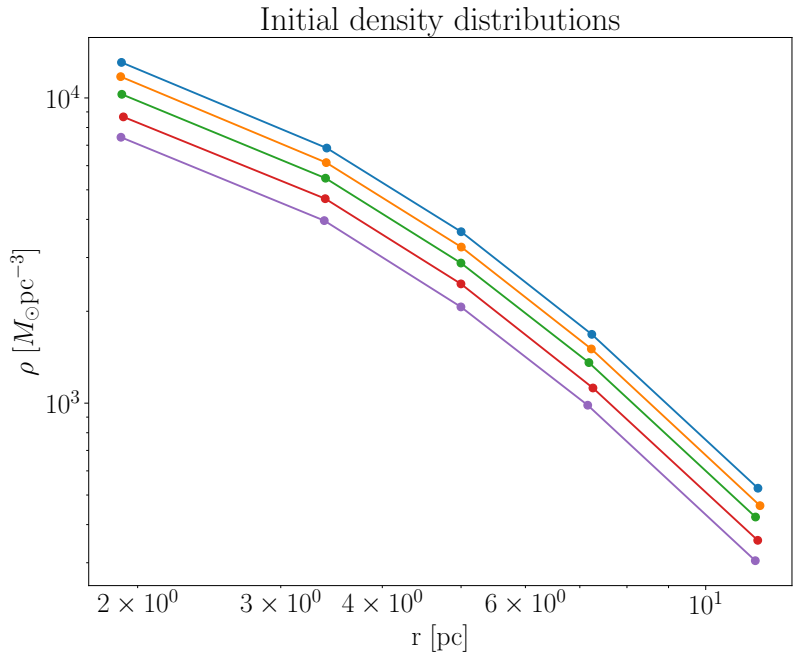

Figure 5.1: Initial density distributions for five simulations with mass scaling from bottom to top (violet solid line: $5 \times 10^5 M_\odot$; red solid line: $6 \times 10^5 M_\odot$; green solid line: $7 \times 10^5 M_\odot$; orange solid line: $8 \times 10^5 M_\odot$; light-blue solud line: $9 \times 10^5 M_\odot$). The distributions reproduce a King profile with $W_0 = 5$ and $r_h = 5$pc.

Mass range [$M_\odot$]	**Simulated time** [Myr]
5×10^5	100
6×10^5	80
7×10^5	30
8×10^5	30
9×10^5	30

Table 5.1: Simulated time of GCs in this work depending on the mass range of the cluster.

Total mass [$M_\odot$]	t_{rlx} [Gyr]	ρ_c [$M_\odot \mathrm{pc}^{-3}$]
515964	3.89	7.09×10^3
614126	4.29	9.15×10^3
718712	4.59	9.78×10^3
813332	4.97	1.07×10^4
911522	5.23	1.39×10^4

Table 5.2: Initial values of the central density and relaxation time of five clusters. The expression used to compute the relaxation time is Eq. 2.5.

5.2 Formation of IMBHs

Out of the ninety simulations run for this work, five of them produced IMBHs. Six IMBHs were the result of stellar mergers in the first ~ 5 Myr of the cluster, and only one was the product of a BBH merger at a later stage (~ 93 Myr). Finally, in two cases the GC hosted two IMBHs.

5.2.1 IMBHs from stellar mergers

All six IMBHs formed before 5 Myr (Fig. 5.4), with a mass of the order of $10^2\, M_\odot$ (Fig. 5.2); the most massive IMBH has a mass of $\sim 229\, M_\odot$. Five out of six IMBHs have $m \leqslant 120\, M_\odot$, falling in the pair-instability mass gap which predicts the absence of BHs with mass between 60 and $120 M_\odot$ [33].
The position of these objects at the time of their formation varies from ~ 2 pc to ~ 10 pc (Fig.5.3); the mass density at the time and position of formation of IMBHs is always within $10^3\, M_\odot \mathrm{pc}^{-3}$.
From the analysis of the *data.mobse.type_change* file it emerges that these IMBHs are the result of the merger between two stars (usually a main-sequence star and a core He-burning star) which are the components of a primordial binary. The merger product continues its evolution as a single star and finally ends its life as a BH. As shown in Appendix A.4, all the *.single*,*.binary* and *.triple* files are studied to obtain a complete picture of the life of the star with the given ID before and after the formation of the IMBH. In all six cases, the IMBHs remained without a companion until the end of the simulation.
Fig. 5.7 shows the evolution of the IMBH positions with time. All the IMBHs

are retained by the end of the simulation (Table 5.1); in particular, the trends show a progressive migration of the compact objects towards the center of the GCs. This result is not surprising, since the higher escape velocities of GCs (up to $v_{esc} \sim 50\text{kms}^{-1}$) lead to the retention of the most massive components of the cluster, which tend to segregate into its core.

The evolution of the binary system leading to the formation of the most massive IMBH is reported in Fig. 5.5. Both binary components are very massive ($m \geqslant 140\,M_{\odot}$) at the beginning and lose a small fraction of mass – probably because of stellar wind – before colliding. As a matter of fact, the fraction of mass lost via stellar winds is negligible at low metallicities ($\dot{M} \propto Z^{\alpha}$), such as the one of the simulated clusters ($Z = 0.0002$). Fig.5.6 shows the stellar evolution of the parent binary system; during its lifetime, the system undergoes two type change processes, contact and a merger.

It is particularly interesting that despite the low central density of the simulated clusters, ranging from 10^3 to $10^4 M_{\odot}\text{pc}^{-3}$, we still observe the formation of IMBHs. These objects have relatively low masses, always in the range of $10^2 M_{\odot}$, and they all originate from a single stellar merger, with one exception (Chap.5.2.2). Massive clusters such as the ones studied in this work, with a large fraction of primordial binaries, can form IMBHs without recurring to long sequences of stellar mergers. It should be noticed however that the initial mass function of the simulated clusters foresees a maximum mass of $150 M_{\odot}$ and that all mergers involve binary systems with small separations ($10^{-7} < a < 10^{-2}$ pc).

The simulations run by Portegies Zwart et al. ([50],[23],[51]) and later by Giersz et al. ([34]) entailed clusters with an high central density ($\rho > 10^6 M_{\odot}\text{pc}^{-1}$) and small relaxation times. In such systems, dynamical encounters would lead to the formation of the most massive stars and, in turn, of the most massive compact remnants. In particular, Giersz proposed that the collisional growth of stars would derive from the existence of a BH sub-cluster at the center of the clusters; in our simulations we found no proof of the existence of such subsystem (Chap. 5.4).
We conclude that massive star clusters ($10^5 - 10^6 M_{\odot}$) with central densities no higher than $10^4 M_{\odot}\text{pc}^{-1}$ and two-body relaxation times as long as a few Gyr (Table 5.2) can experience the formation of IMBHs from the stellar evolution of primordial hard binaries.

5.2.2 IMBHs from binary black hole mergers

Only one IMBH results from the merger of two stellar-mass BHs; the host GC has a mass $m_{CL} \sim 5.76 \times 10^5 M_{\odot}$. Specifically, the BBH is the outcome of the evolution of a primordial binary with initial masses $m_1 \sim 65 M_{\odot}$ and

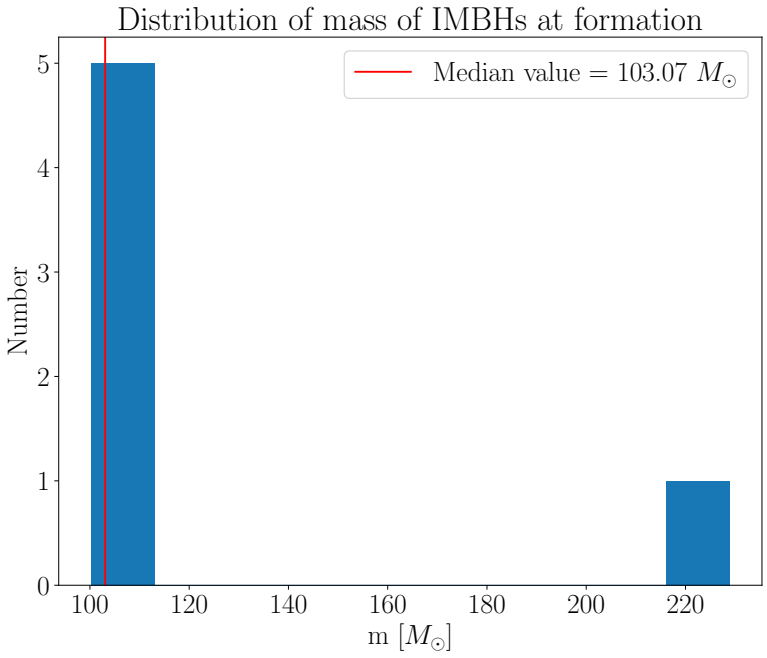

Figure 5.2: Mass distribution of IMBHs at their formation.

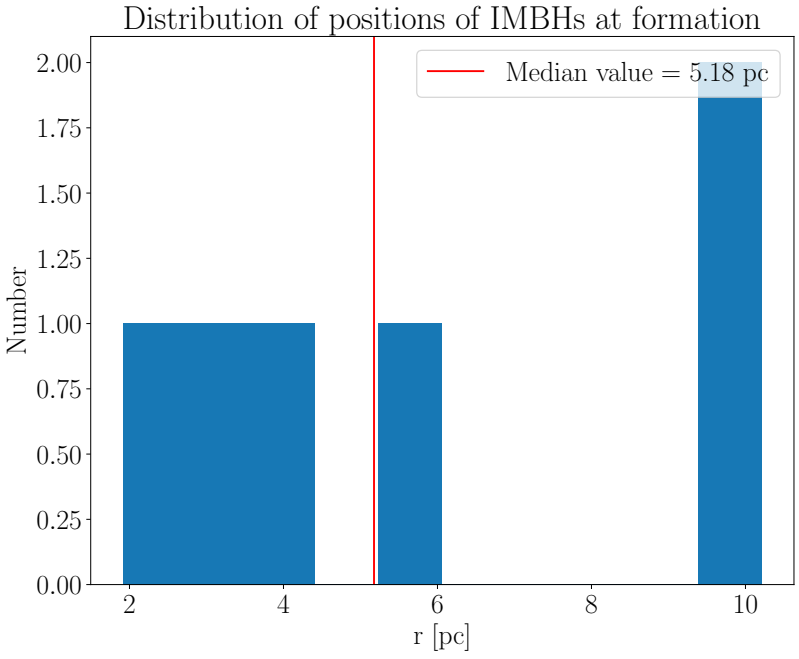

Figure 5.3: Distribution of the distances of IMBHs from the center of the star cluster at the time of their formation.

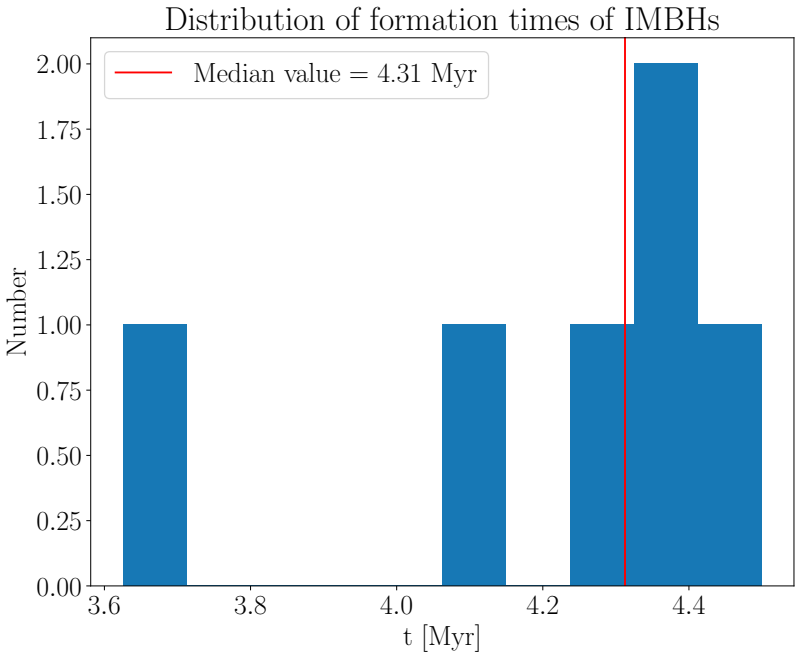

Figure 5.4: Distribution of IMBH formation times.

$m_2 \sim 42M_\odot$ (Fig.5.8); the system was born with low eccentricity (0.15–0.175) and a small semi-major axis ($\leqslant$ 0.0035 pc). The binary sinks towards the central regions of the cluster, and the merger takes place at $r \sim 1$ pc. Shortly after coalescence (t$\sim$ 93 Myr), the IMBH enters a triple system, perturbing a BBH with masses $m_1 \sim 33.5M_\odot$ and $m_2 \sim 26M_\odot$. The IMBH continues to migrate towards the center of the cluster until the end of the simulation (Fig.5.9).

From a further integration of this cluster, we might observe an exchange between the IMBH and the least massive binary component; this could lead to the hardening of the binary system, and eventually to a merger. In order to confirm a slow mass accretion mechanism of the IMBH in the cluster core, as the one predicted by Miller and Hamilton [52], we would need a longer integration time.

Finally, it is particularly interesting that this IMBH forms in a cluster already containing another IMBH with $m \sim 105M_\odot$, resulting from stellar mergers. Another cluster with $m_{CL} \sim 7.66 \times 10^5 M_\odot$ hosts two IMBHs both originated from stellar mergers. In the end, this could lead to the creation of a IMBH-IMBH binary as foreseen by Gurkan [68] in the case of massive systems with a low concentration ($W_0 = 3$).

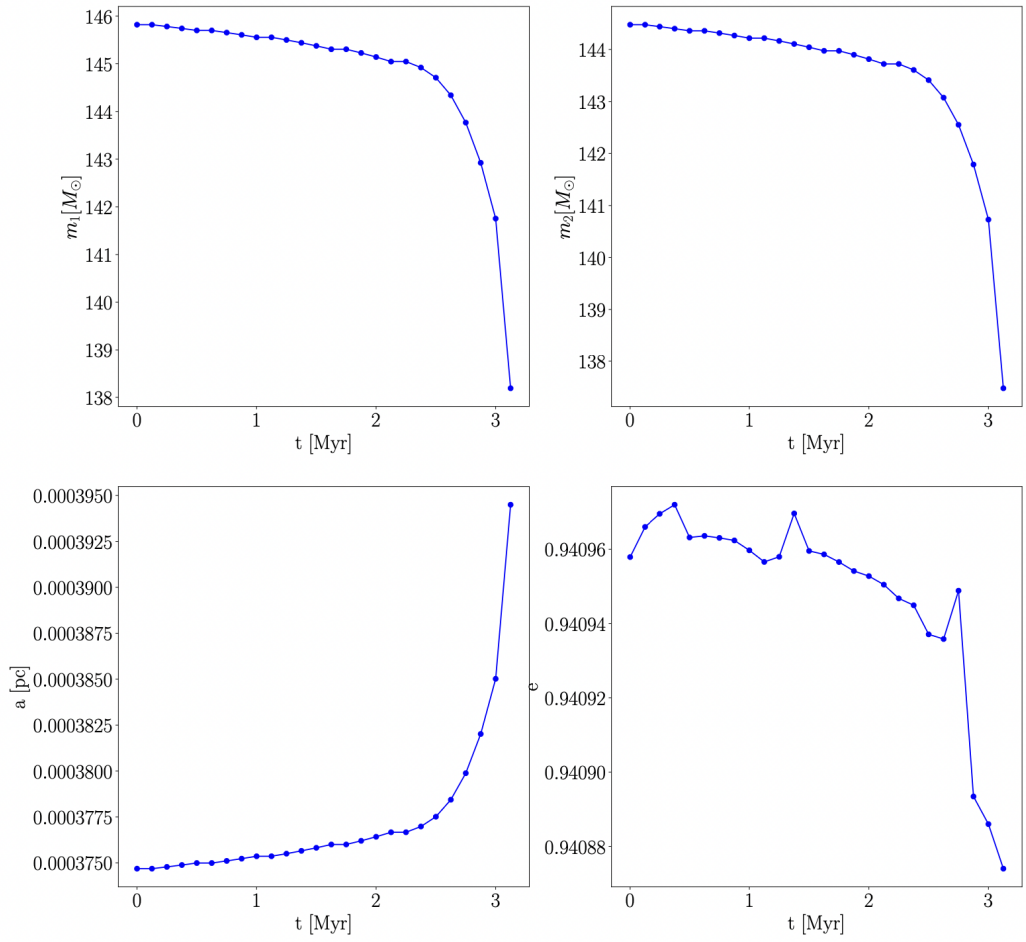

Figure 5.5: Evolution of the binary system leading to the formation of the most massive IMBH in the simulations. *Top panel*: evolution of m_1 and m_2; *bottom panel*: evolution of the semi-major axis (a) and of the eccentricity (e) of the system. During the first ~ 3 Myr, the binary components are both main sequence stars.

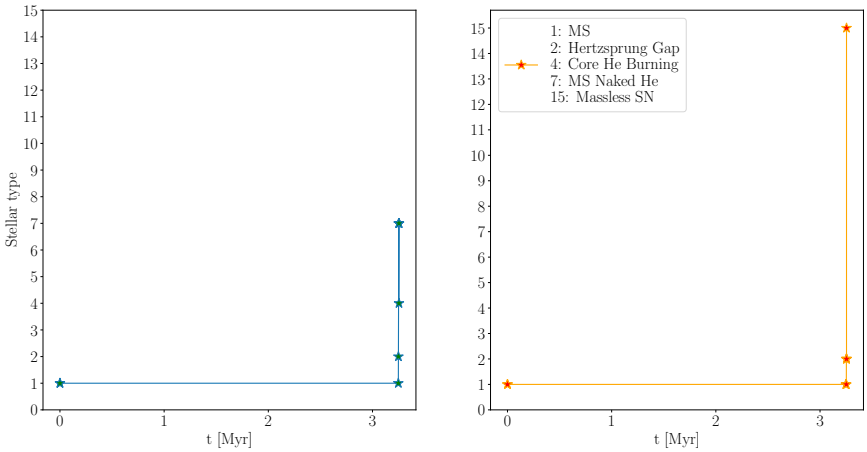

Figure 5.6: Stellar evolution of the binary components leading to the formation of the most massive IMBH in the simulations. On the left the evolution of the primary: main sequence → Hertzsprung gap → main sequence naked-helium star → core-helium burning star. On the right the evolution of the secondary: main sequence → Hertzsprung gap → massless supernova. The stellar types were tracked analysing the *data.mobse.type_change* file.

5.3 Black holes and binary black holes

5.3.1 Properties of black holes

The dynamical evolution of GCs is dominated by the fate of their compact objects, which could either be retained or ejected by their host cluster.
We retrieved the fraction of BHs escaping the cluster with respect to the total number of BHs at each time. This was possible by using the `PeTar` tools *petar.SingleEscaper()* and *petar.BinaryEscaper()*. Fig.5.10 shows that throughout the duration of the simulations, the fraction of BHs escaping the clusters is always less than 8%. As a matter of fact, the typical escape velocity of GCs is $\sim$ 50kms^{-1}, higher than the escape velocities in open and young star clusters; this leads to an higher fraction of retained BHs [25]. It should be noticed that in the present calculations we have not taken into account the contribution of relativistic kicks (Chap.2.3) that could lead to a larger number of ejected BHs; as a consequence, the present results should be considered as a lower limit to the number of escaping BHs in young GCs.

In Fig.5.10 a first spike is seen around 10 Myr and a second bump between $\sim$20 and 40 Myr. From a comparison with Fig.5.11, it is possible to notice that the first 10 Myr correspond to a steep rise in the number of BHs in the simulated clusters; as a matter of fact, in this period we expect the formation of BHs from the stellar evolution of massive stars. In the period of time until $\sim$40

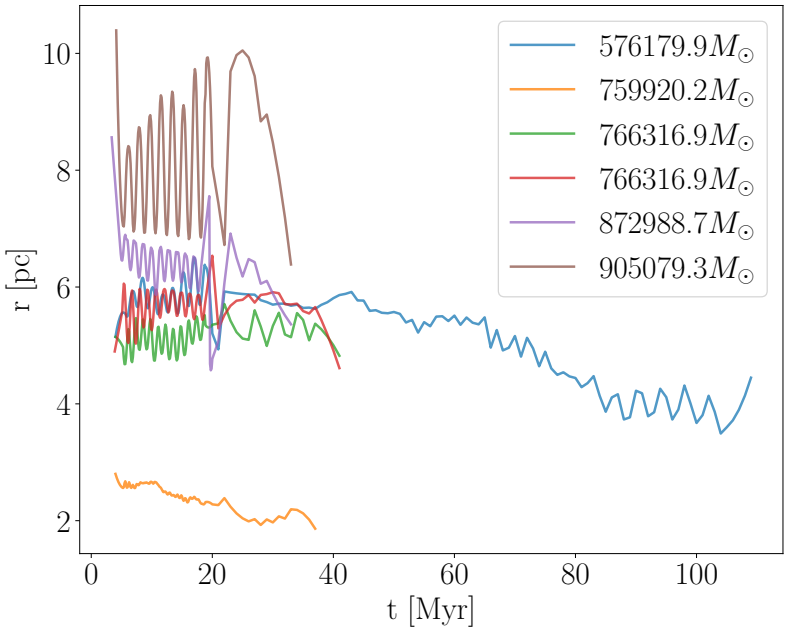

Figure 5.7: Evolution of the position of the six IMBHs deriving from stellar mergers inside their clusters; the trends are averaged to provide a better visualization. It appears that the IMBHs are slowly migrating towards the center of their host clusters; this behaviour is particularly clear in the case of the least massive cluster (blue solid line).

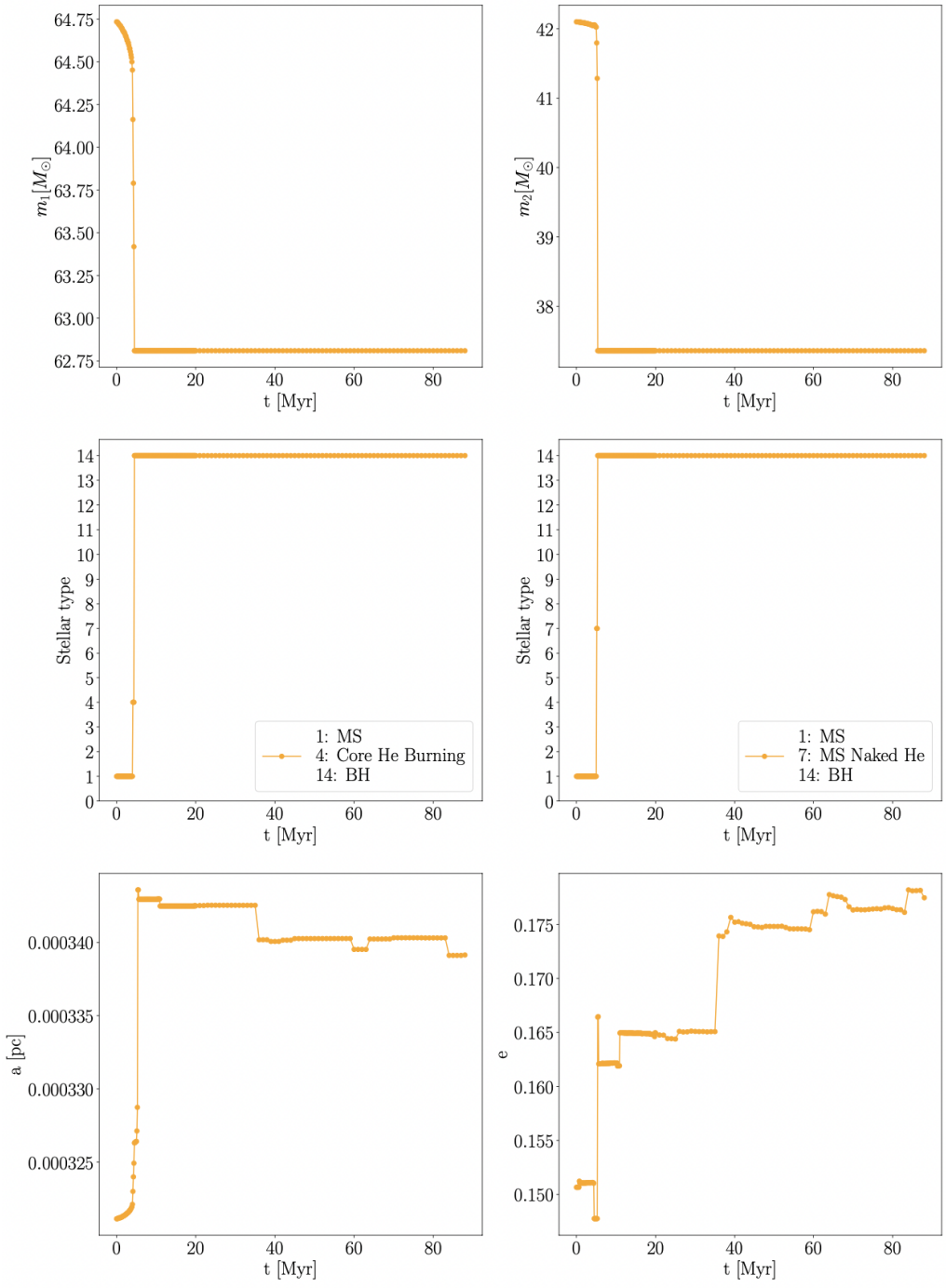

Figure 5.8: Evolution of the binary system resulting into the BBH whose merger creates an IMBH. *Top panel*: evolution of m_1 and m_2; *central panel*: stellar types of the binary components with time; *bottom panel*: evolution of the semi-major axis (a) and the eccentricity (e) of the binary system.

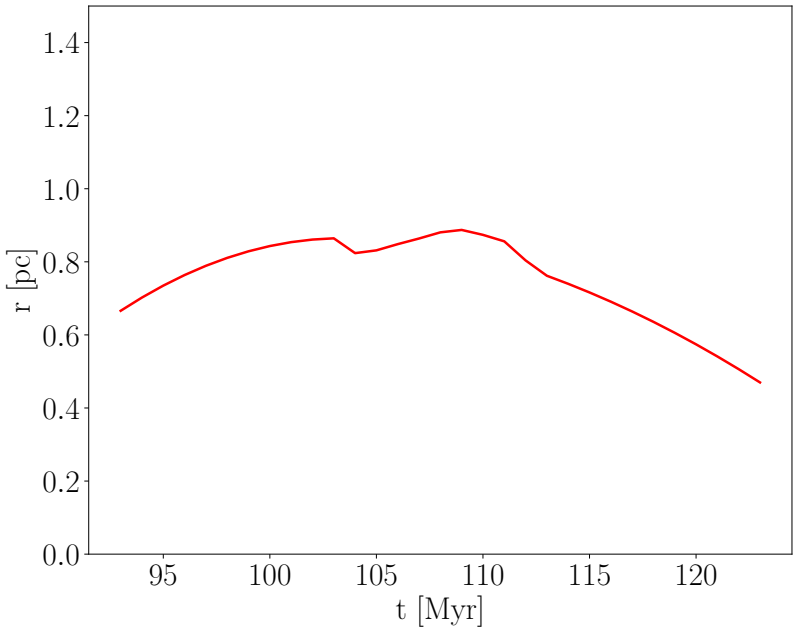

Figure 5.9: Evolution of the position of the IMBH resulting from the BBH merger. During this time, the compact object is found in a triple system. The position is averaged to provide a better visualization.

Myr, the slope decreases, and it finally reaches a plateau. The first bump in the number of ejected BHs corresponds to the compact objects ejected at the moment of their creation from a strong supernova kick. In the next $\sim$ 30Myr, the creation of BHs continues at a slower rate, and the massive compact objects steadily migrate towards central, dense regions of the cluster, leading to dynamical encounters and to a second bump in the number of escaping BHs. The average mass of the ejected BHs is $\sim 15 M_{\odot}$.
The small fraction of ejected BHs, combined with the effect of the dynamical friction, could eventually lead to the formation of BH sub-clusters at the center of the simulated clusters.

5.3.2 Properties of binary black holes

It is useful to study the general properties of the BBHs in the simulated clusters in order to obtain a clearer picture of the dynamical state of the GCs ([69],[25]). In particular, we have analysed the distribution of primary and secondary masses in merging BBHs, i.e. BBHs that reach coalescence within a Hubble time (Fig. 5.12). We did not notice any correlation between the BH masses and the mass of the host star clusters; massive BBHs form both in low-mass ($5 \times 10^5 M_{\odot}$) and in high-mass ($9 \times 10^5 M_{\odot}$) star clusters.
On the other hand, the number of merging BBHs increases with the cluster mass; even though the simulation time for the heavier clusters has reached a maximum of $\sim$ 30Myr, Fig.5.12 shows a larger number of merging objects in the GCs with $m_{CL} > 7 \times 10^5 M_{\odot}$. GCs within the mass range of $9 \times 10^5 M_{\odot}$ show a lower number of BBH mergers which is probably due to the lower number of simulated clusters in such range.

From the information on the masses of merging BBHs it is possible to plot the mass of the secondary BH m_2 versus the mass of the primary BH m_1 in merging BBHs (Fig. 5.13). The most massive objects ($m_1 > 45 M_{\odot}$) result from the evolution of primordial binaries. The choice of this threshold at $45 M_{\odot}$ derives from [6] in which it is indicated that the mass distribution of the primary BH in the observations made by the LIGO–Virgo Collaboration during the first two observing runs can be approximated by models with $\leqslant 1\%$ BHs more massive than $45 M_{\odot}$. In our simulations of young GCs, these BBH mergers arise from the evolution of primordial binary systems, accounting for 0.7% of the total number of BBH mergers.

In addition, we computed the merger efficiency η as a function of the cluster mass range. This quantity is defined as

$$\eta = \frac{N_{merge}}{M_*}$$

with N_{merge} the total number of merging BBHs and $M_* = \sum_i m_{CL,i}$, with the index i running over the clusters in a given mass range. The merger efficiency

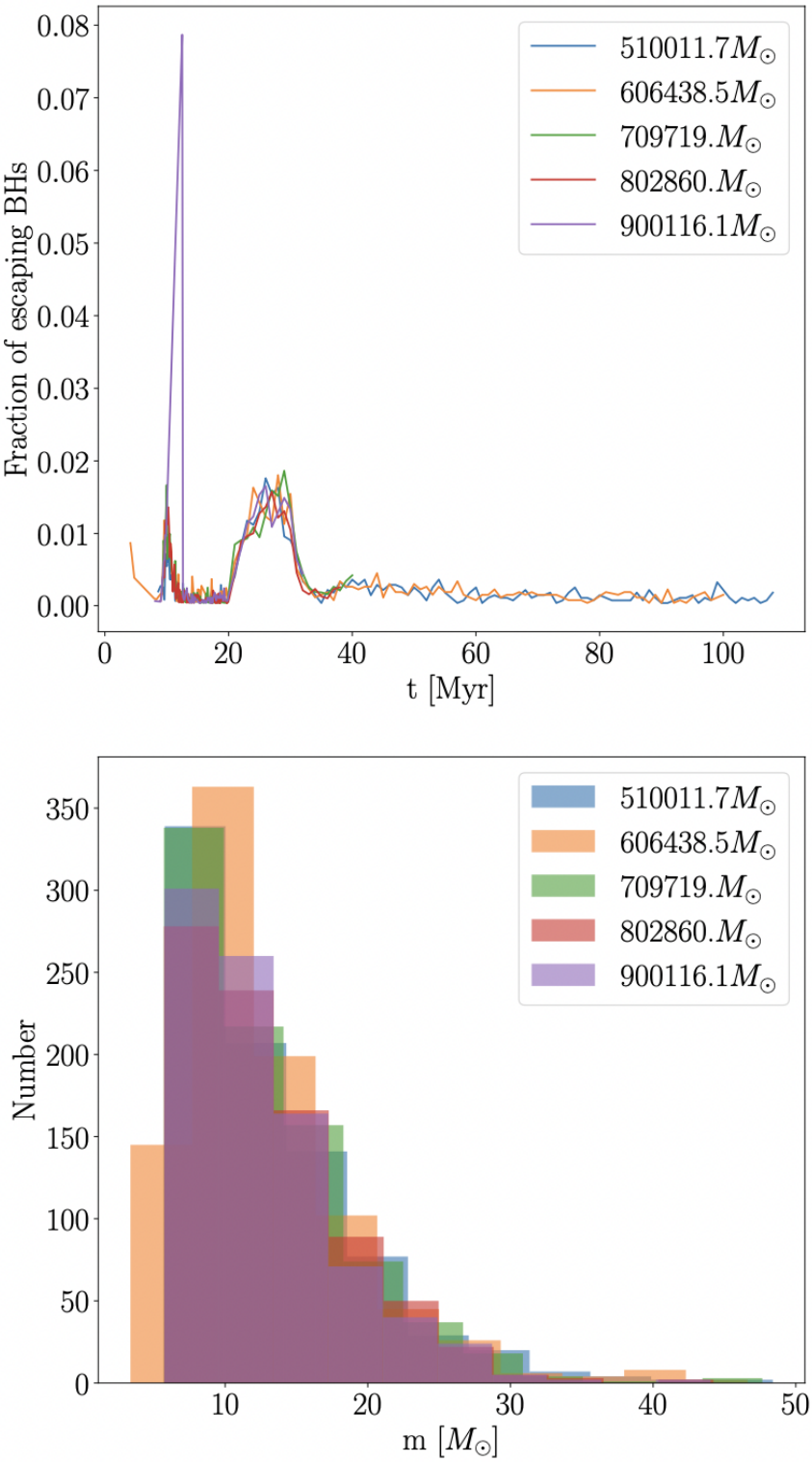

Figure 5.10: *Top panel*: fraction of escaping BHs (either single or in a binary) with respect to the total number of BHs at that time. *Bottom panel*: mass distribution of escaping BHs. The trends are representative for the five mass ranges.

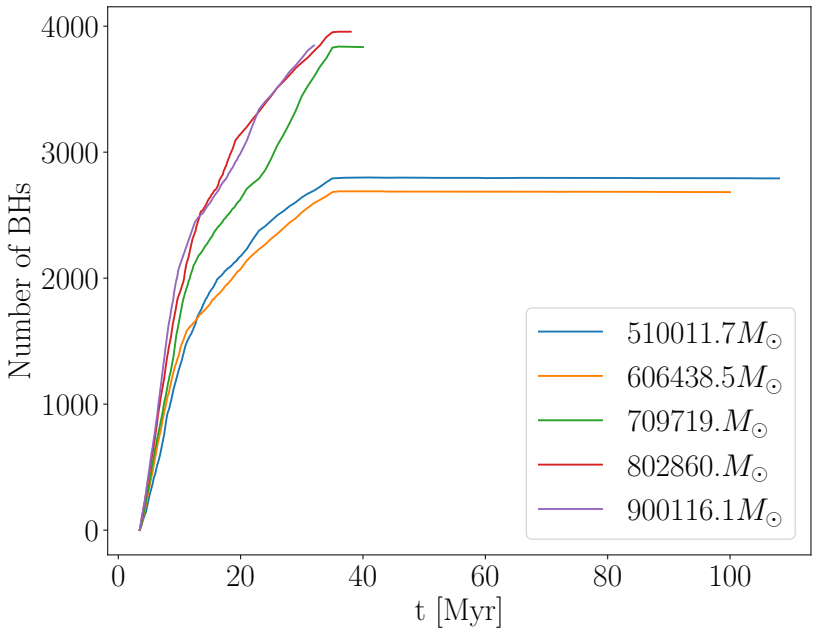

Figure 5.11: Time evolution of the number of BHs (either single or in a binary system).

is a good proxy for the merger rate, since it does not depend on the star formation rate and metallicity evolution of the Universe.
The results of the calculations are found in Table 5.3. η decreases with increasing cluster mass; this outcome may be due to the smaller simulation time of the most massive GCs, and it will be fully explored in future works. As a matter of fact, the dynamical timescales of systems as massive as $10^6 M_\odot$ are long, and so far we have only been able to analyse the properties of young GCs, while still dominated by stellar evolution.

Mass range $[M_\odot]$	**Merger efficiency** $\eta[M_\odot^{-1}]$
5×10^5	1×10^{-4}
6×10^5	9.13×10^{-5}
7×10^5	6.8×10^{-5}
8×10^5	6.14×10^{-5}
9×10^5	5.52×10^{-5}

Table 5.3: Merger efficiency η in the simulated clusters depending on their mass range.

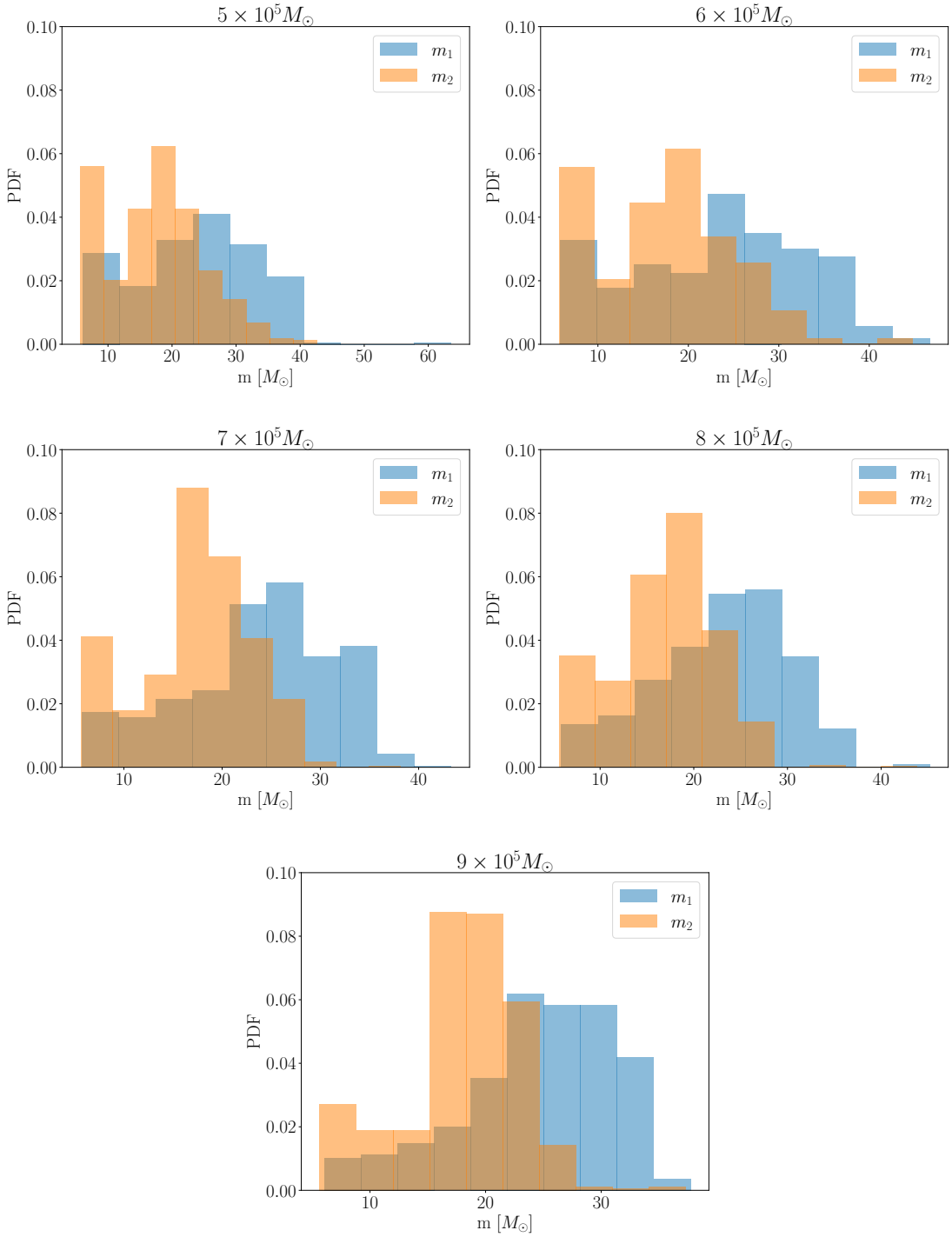

Figure 5.12: Distribution of primary (m_1) and secondary (m_2) mass of all merging BBHs.

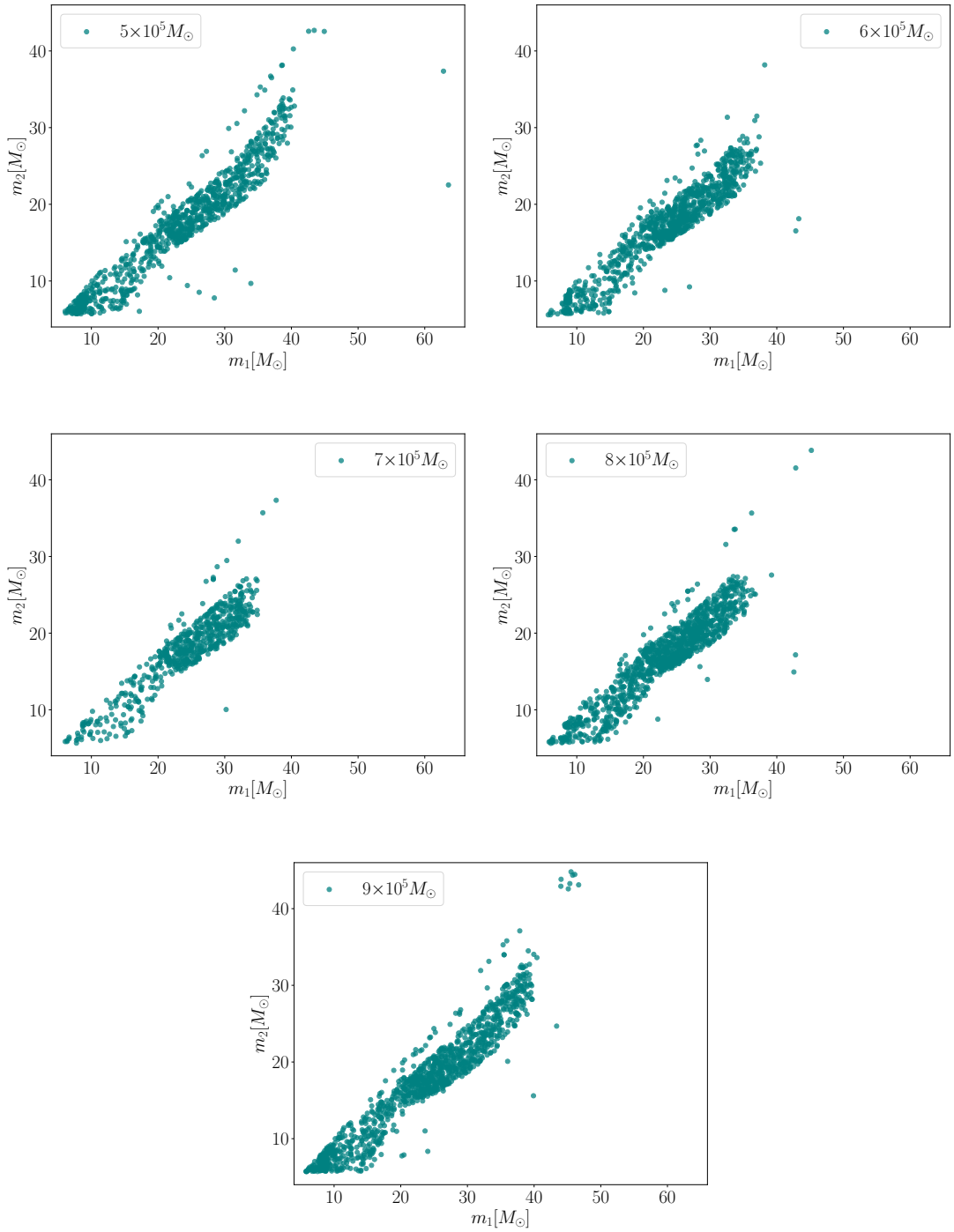

Figure 5.13: Mass of the primary BH (m_1) versus mass of the secondary BH (m_2) of merging BBHs in the five host cluster mass ranges (5×10^5–$9\times10^5 M_\odot$).

5.4 Black hole sub-cluster

In order to understand whether a BH sub-cluster forms at the center of the simulated GCs in this first evolutionary phase, we analysed the evolution of the central density of stars and compared it to the central density due to BHs only.

This was possible thanks to the *petar.LagrangianMultiple()* tool, which allows to retrieve the Lagrangian and core properties for various stellar types at once, after having specified them during the processing of data.
It was found that in no cluster there is indication for a larger BH central density. Fig.5.14 shows the evolution of the density at the center of a GC with mass $\sim 6 \times 10^5 M_\odot$; the density due to all the stellar types decreases with time, while simultaneously there is an increase in the BH density. After ∼80 Myr the former quantity stabilizes, while the latter one shows a slight but steady growth.

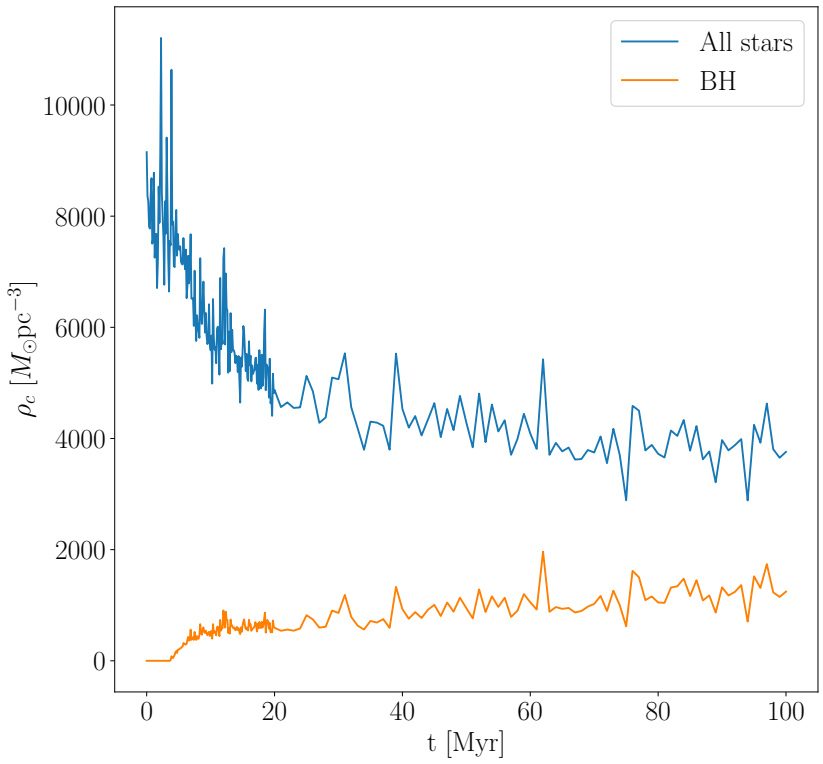

Figure 5.14: Evolution of the central density of all stars and BHs only during the first 100 Myr of the cluster. The mass range of the analysed cluster is $6 \times 10^5 M_\odot$.

5.5 Lagrangian radii

In Fig.5.15 we show the evolution of the Lagrangian radii containing 10, 30, 50, 70 and 90% of the cluster mass. From a comparison between the two trends, one of which related to clusters with IMBHs and the other to clusters with no IMBHs, it would appear that GCs with two IMBHs expand more rapidly than GCs with no central compact object. This behaviour is not observed when the cluster contains only one IMBH.
This result is anyways partial and it could be the product of a poor statistics on clusters with one or more IMBHs.

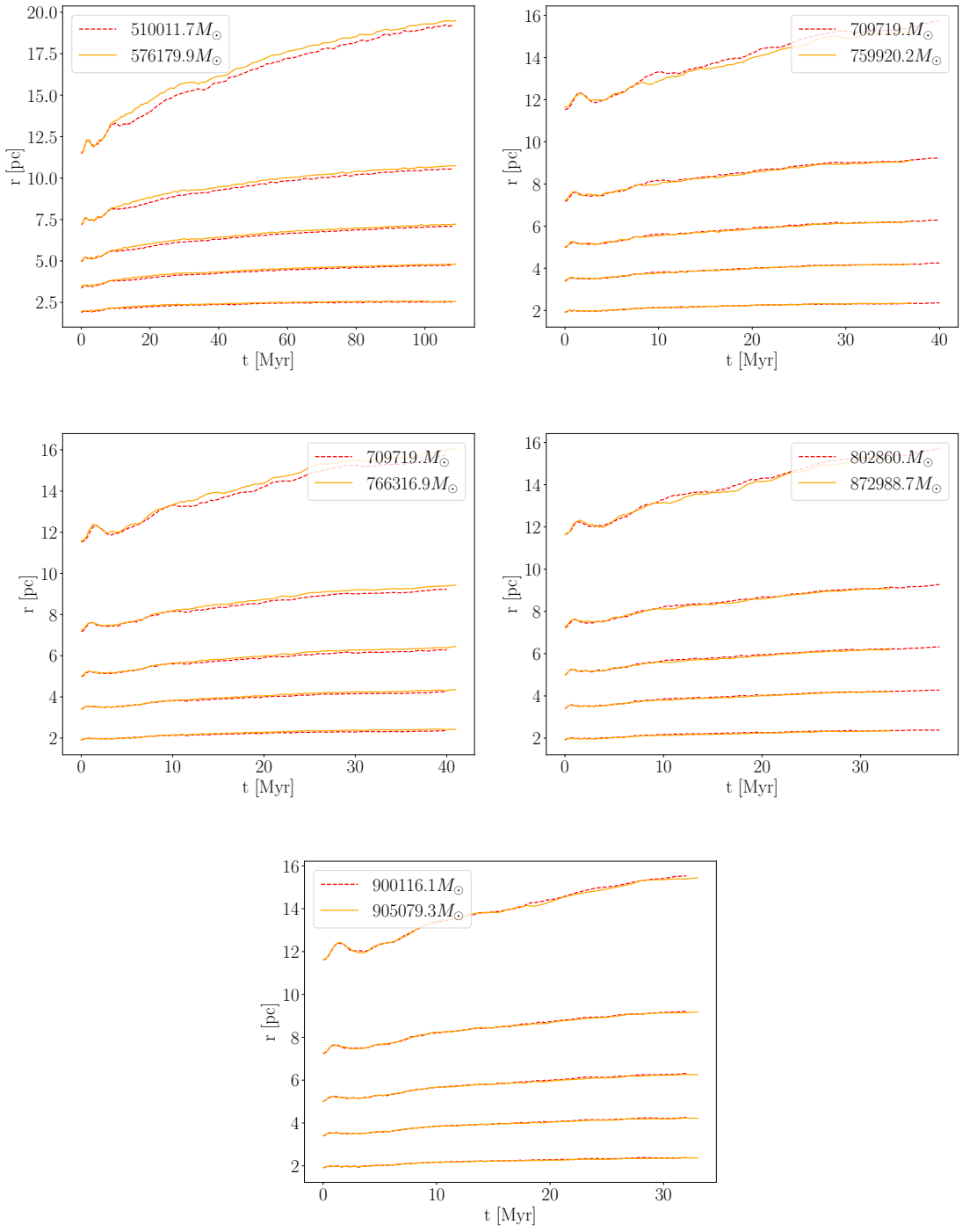

Figure 5.15: Evolution of the Lagrangian radii of nine simulated clusters; the dashed red line corresponds to a cluster containing IMBHs, the orange solid line is instead related to a cluster with no IMBHs. From the bottom to the top the trends of the radii containing 10%, 30%, 50%, 70% and 90% of the cluster mass are shown.

Chapter 6

Conclusions

The purpose of this work is the analysis of the formation processes and main properties of IMBHs in young, dense, massive star clusters. We found that the main formation channel of such objects is the evolution of a stellar merger product in the first $\sim$ 5 Myr of the cluster life. All the colliding stars were the components of primordial binaries. Only one IMBH resulted from a BBH merger. All IMBHs have a mass of the order of $10^2 M_{\odot}$. In two simulated clusters, we found evidence for two IMBHs; in one case, they were both the result of stellar mergers, in the other, one was the result of a stellar merger and the other of a BBH merger. The slow migration of such objects towards the center of the cluster observed in our data might lead to the creation of a IMBH-IMBH binary, as speculated by Gurkan [68]. None of the IMBHs found in the simulated clusters was ejected from the host GC during the time of the simulation.

We also studied the properties of the BHs and BBHs of the simulated clusters, with a focus on the properties of merging BBHs. We found that the distribution of primary and secondary masses of merging BBHs does not depend on the mass of the GC, while an higher number of mergers is found at larger cluster masses. Fig. 5.12 shows the primary versus secondary mass of merging BBHs; primaries with a mass larger than $45 M_{\odot}$ formed in primordial binary systems. From the total number of BBH mergers, we were also able to draw the merger efficiency η, which appears to decrease with increasing mass of the cluster; this outcome could be the result of a shorter time of integration in the case of heavier clusters. It should be noticed that the simulations are still running, and that we plan to integrate all of our clusters up to 10 Gyr.

We also retrieved the properties of escaping BHs (either belonging to a binary system or single). The fraction of retained BHs in our clusters is very high, with a maximum of 8% of ejected BHs throughout the duration of the simulations. The average mass of the escaping BHs is around $\sim 15 M_{\odot}$, in line with the idea that heavier compact objects tend to be retained by their host GC.

We searched for the presence of a BH sub-cluster at the center of the simulated GCs. By comparing the central density of stars and that of BHs only, we did not find evidence for a central BH overdensity. Because of the large number of retained BHs, and as a consequence of their migration towards the cluster center, such a subsystem could develop in the future.

Finally, we performed an analysis of the evolution of the Lagrangian radii. In the two cases in which the cluster hosts two IMBHs, the cluster expands more rapidly than if there were none. In order to confirm such result, a more thorough study will have to be performed.

The results found in this work will be further explored in a future paper. The simulated time will reach at least 1 Gyr and lead to more decisive results regarding the fate of IMBHs in GCs (whether they are ejected, their final masses, the possibility of the formation of a IMBH-BH or IMBH-IMBH binary).
We will also estimate the merger efficiency and the BBH merger rate; these quantities are essential in the context of GW observations. In order to provide a better modeling of GW emissions from compact objects in dense, massive star clusters, the knowledge of the properties (especially the mass range) and number of merging BBHs in such systems is essential.
Moreover, the formation rate of IMBHs in GCs will be useful to both LISA and the Einstein Telescope [7], which will work in the frequency band of the mergers between IMBHs or between an IMBH and a stellar-mass BH.

Appendices

Appendix A

Scripts

A.1 Example of job file submitted to MARCONI100

```
#!/bin/bash
#SBATCH --time=23:59:00   ##maximum time of the run
#SBATCH --job-name=RUN_0
#SBATCH --nodes=1   ##number of nodes requested
#SBATCH --ntasks-per-node=1   ##number of MPI processes


#SBATCH -p m100_usr_prod   ##name of the partition


#SBATCH --cpus-per-task=64   ##number of logical CPUs requested


#SBATCH --gres=gpu:1   ##number of requested GPUs


#SBATCH --output=mpi.out.0
#SBATCH --error=mpi.err.0


#SBATCH --account=INF22_virgo_0   ##name of the project

export OMP_NUM_THREADS=64

export OMP_PROC_BIND=spread #OMP threads are spread on the hardware threads of the physical cores

#indicating paths where the codes are found
export PYTHONPATH=$PYTHONPATH:/m100/home/userexternal/bmestich/code/executables/include
export PATH=$PATH:/m100/home/userexternal/bmestich/code/executables/bin
```

```
30     export OMP_STACKSIZE=128M
31
32     bash  loop0.sh  #the loop file contains all the commands
       needed to generate the initial conditions and run the
       simulation
```

A.2 Example of loop file

```
#!/bin/bash
arrayA=(509641.7) #initial mass of the cluster
for mcl in ${arrayA[*]};
    do
    echo "$mcl"
    cd /m100_scratch/userexternal/bmestich/SIM_0.0002
    mkdir -p s"$mcl"
    cd s"$mcl"

#generating initial conditions with mcluster
./mcluster -M "$mcl" -R 5 -P 1 -W 5 -C 5 -G 1 -f 2 -a -1.3
-a -2.3 -m 0.1 -m 0.5 -m 150 -b 0.4 -e 0 -Z 0.0002 -t 1 -u 1

#matching observational results by sana 2012 and moe & di
stefano 2017
python light_multiplet_recombinator_py3.py > logbin

#obtain the number of primordial binaries
var=$(grep "2\.35" input | awk {"print $4"})

#write the initial conditions in format readable by PeTar
./petar.init -v kms2pcmyr -s mobse -c 8000,0,0,0,220,0 -t
dat.10

#start simulation
./petar --mobse-metallicity 0.0002 --mobse-nsflag 2 --mobse
-alpha 1 --mobse-bhflag 3 --mobse-lambda 0.1  -u 1  -t 20 -b
 "$var" -o 0.125 --galpy-type-arg
15,5,9:0.0299946,1.8,0.2375,0.7574802,0.375,0.035,4.85223053,2.0
   dat.10.input > log.petar0

cd /m100_scratch/userexternal/bmestich/SIM_0.0002
```

A.3 Code identifying IMBHs in the PeTar output files

```
import petar
import numpy as np
import os

p = petar.Particle(interrupt_mode='mobse',external_mode='galpy')

#only the unprocessed data files are analysed (in the first 20 Myr they are produced every 0.125 Myr, afterwards every 1 Myr)

files = []
for i in os.listdir('./'):
    if i.startswith('data') and not 'esc' in i and not 'group' in i and not 'mobse' in i and not 'mosse' in i and not 'rank' in i and not 'status' in i and not 'snap' in i:
        files.append(i)
files = sorted(files, key=lambda x: int(x[5:]))

id_imbh = []

for i in range(0,160,10): #for the first 20 Myr the check is executed every 1.25 Myr
    p.loadtxt(files[i], skiprows=1)
    bh = p.star.type==14
    imbh = p.star.mass[bh]>100
    ids = p.id[bh][imbh]
    if len(ids)>0:
        print(f'Found IMBH with ID {ids} at time {int(files[i][5:])*0.125} Myr')
        for i in range(len(ids)):
            if ids[i] not in id_imbh:
                id_imbh.append(ids[i])

for i in range(160,len(files)+1,5): #after the first 20 Myr the check is done every 5 Myr
    p.loadtxt(files[i], skiprows=1)
    bh = p.star.type==14
    imbh = p.star.mass[bh]>100
    ids = p.id[bh][imbh]
    if len(ids)>0:
        print(f'Found IMBH with ID {ids} at time {int(files[i][5:])-140} Myr')
        for i in range(len(ids)):
            if ids[i] not in id_imbh:
                id_imbh.append(ids[i])

print(id_imbh) #IDs of the IMBHs

```

```
41 #analyse binary evolution of star resulting in IMBH
42 ty = petar.BSETypeChange()
43 ty.loadtxt('data.mobse.type_change')
44
45 #check whether the IMBH is result of hyperbolic/dynamic merger
46 if os.path.getsize('data.mobse.dynamic_merge')>0:
47     dy = petar.BSEDynamicMerge()
48     dy.loadtxt('data.mobse.dynamic_merge')
49
50 #obtain binary/single SN kick received by IMBH (if any)
51 bsn = petar.BSESNKick()
52 bsn.loadtxt('data.mobse.sn_kick')
53
54 sn = petar.SSESNKick()
55 sn.loadtxt('data.mosse.sn_kick')
56
57
58 for i in range(len(id_imbh)):
59     mask = (ty.id1==id_imbh[i]) | (ty.id2==id_imbh[i])
60     k = ty.type[mask] #binary evolution type change
61     z = np.zeros(shape=(len(k),12))
62     z[:,0] = ty.id1[mask]
63     z[:,1] = ty.id2[mask]
64     z[:,2] = k
65     z[:,3] = ty.init.time[mask]
66     z[:,4] = ty.init.type1[mask] #initial type of primary
67     z[:,5] = ty.init.type2[mask] #initial type of secondary
68     z[:,6] = ty.final.type1[mask] #final type of primary
69     z[:,7] = ty.final.type2[mask] #final type of secondary
70     z[:,8] = ty.init.m1[mask] #initial mass of primary
71     z[:,9] = ty.init.m2[mask] #initial mass of secondary
72     z[:,10] = ty.final.m1[mask] #final mass of primary
73     z[:,11] = ty.final.m2[mask] #final mass of secondary
74     np.savetxt(f'type_changes_{id_imbh[i]}.txt',z)
75
76     if os.path.getsize('data.mobse.dynamic_merge')>0:
77         mask1 = (dy.id1==id_imbh[i]) | (dy.id2==id_imbh[i])
78             if len(dy.init.p1.time[mask1])>0:
79                 print('Check dynamic merger!')
80
81     mask2 = (bsn.id1==id_imbh[i]) | (bsn.id2==id_imbh[i])
82     if len(bsn.vkick[mask2])>0:
83         print(f'Velocity of SN kick in binary system:{bsn.vkick
    [mask2]}')
84
85     mask3 = (sn.id==id_imbh[i])
86     if len(sn.vkick[mask3])>0:
87     if len(sn.vkick[mask3])>0:
88       print(f'Velocity of SN kick:{sn.vkick[mask3]}')
```

A.4 Code analysing evolution of IMBH as a single star, in a binary or in a triple system

```
import petar
import os
import numpy as np

p = petar.Particle(interrupt_mode='mobse', external_mode='galpy') #single particle

p1 = petar.Particle(interrupt_mode='mobse', external_mode='galpy')
p2 = petar.Particle(interrupt_mode='mobse', external_mode='galpy')
binary = petar.Binary(p1,p2) #binary particle

triple = petar.Binary(member_particle_type_one=petar.Particle, member_particle_type_two=[petar.Particle, petar.Particle], interrupt_mode='mobse', external_mode='galpy') #triple system

files_s = []
files_b = []
files_t = []
for f in os.listdir('./'):
    if f.endswith('.single') and f.startswith('data'):
        files_s.append(f)
    elif f.endswith('.binary') and f.startswith('data'):
        files_b.append(f)
    elif f.endswith('.triple') and f.startswith('data'):
        files_t.append(f)
files_s = sorted(files_s, key=lambda x: int(x[5:-7]))
files_b = sorted(files_b, key=lambda x: int(x[5:-7]))
files_t = sorted(files_t, key=lambda x: int(x[5:-7]))
print(files_t)
id_imbh = 161 #id of IMBH found with previous code

#single files analysis
print('Single analysis')
m_s = []
t_s = []
r_s = []
k_s = []
for i in files_s: #life of star with id_imbh as single
    fileb = i
    p.loadtxt(fileb)
    single_id = (p.id==id_imbh)

    m = p.star.mass[single_id]
    if len(m)>0:
```

```
42          m_s.extend(m) #mass of single star
43          r_s.extend(p.star.rad[single_id]) #radius of single
    star
44          k_s.extend(p.star.type[single_id]) #stellar type of
    single star
45          print(f'data {fileb[5:-7]}')
46          if int(fileb[5:-7])<=160:
47              t_s.append(int(fileb[5:-7])*0.125) #time from birth
     of cluster
48          elif int(fileb[5:-7])>160:
49              t_s.append(int(fileb[5:-7])-140)
50 if len(m_s)>0:
51      z = np.zeros(shape=(len(m_s),4))
52      z[:,0] = t_s
53      z[:,1] = m_s
54      z[:,2] = r_s
55      z[:,3] = k_s
56      np.savetxt(f'single_{id_imbh}.txt',z)
57
58 #binary analysis
59 print('Binary analysis')
60 M1 = []
61 M2 = []
62 t_b = []
63 a = []
64 e = []
65 k1 = []
66 k2 = []
67 id1 = []
68 id2 = []
69 for i in files_b: #life of star with id_imbh in a binary
70      fileb = i
71      binary.loadtxt(fileb)
72      bin_id = (binary.p1.id==id_imbh) | (binary.p2.id==id_imbh)
    #star with id_imbh could be either primary or secondary
73      m1 = binary.p1.mass[bin_id] #mass of primary
74      m2 = binary.p2.mass[bin_id] #mass of secondary
75
76      if len(m1)>0 and len(m2)>0:
77          M1.extend(m1)
78          M2.extend(m2)
79          a.extend(binary.semi[bin_id]) #semi-major axis of
    binary
80          e.extend(binary.ecc[bin_id]) #eccentricity of binary
81          k1.extend(binary.p1.star.type[bin_id]) #stellar type of
     primary
82          k2.extend(binary.p2.star.type[bin_id]) #stellar type of
     secondary
83          id1.extend(binary.p1.id[bin_id]) #id of primary
84          id2.extend(binary.p2.id[bin_id]) #id of secondary
85          print(f'data {fileb[5:-7]}')
86          if int(fileb[5:-7])<=160:
87              t_b.append(int(fileb[5:-7])*0.125) #time from birth
```

```
      of cluster
88          elif int(fileb[5:-7])>160:
89              t_b.append(int(fileb[5:-7])-140)
90 if len(M1)>0:
91     z = np.zeros(shape=(len(M1),9))
92     z[:,0] = id1
93     z[:,1] = id2
94     z[:,2] = t_b
95     z[:,3] = M1
96     z[:,4] = M2
97     z[:,5] = k1
98     z[:,6] = k2
99     z[:,7] = a
100    z[:,8] = e
101    np.savetxt(f'binary_{id_imbh}.txt',z)
102
103 #triple analysis
104 print('Triple analysis')
105 ms = []
106 mb1 = []
107 mb2 = []
108 ks = []
109 k1 = []
110 k2 = []
111 t_t = []
112 ids = []
113 id1 = []
114 id2 = []
115 for i in files_t: #life of star with id_imbh in triple system
116     fileb = i
117     triple.loadtxt(fileb)
118     tr_id = (triple.p1.id==id_imbh) | (triple.p2.p1.id==id_imbh
    ) | (triple.p2.p2.id==id_imbh) #star with id_imbh could be
    either perturber/primary/secondary
119
120     m = triple.p1.star.mass[tr_id] #mass of single perturber
121     m1 = triple.p2.p1.star.mass[tr_id] #mass of primary
122     m2 = triple.p2.p2.star.mass[tr_id] #mass of secondary
123     if len(m)>0 and len(m1)>0 and len(m2)>0:
124         ms.extend(m)
125         mb1.extend(m1)
126         mb2.extend(m2)
127         ks.extend(triple.p1.star.type[tr_id]) #stellar type of
    perturber
128         k1.extend(triple.p2.p1.star.type[tr_id]) #stellar type
    of primary
129         k2.extend(triple.p2.p2.star.type[tr_id]) #stellar type
    of secondary
130         ids.extend(triple.p1.id[tr_id]) #id of single perturber
131         id1.extend(triple.p2.p1.id[tr_id]) #id of primary
132         id2.extend(triple.p2.p2.id[tr_id]) #id of secondary
133         if int(fileb[5:-7])<=160:
134             t_t.append(int(fileb[5:-7])*0.125) #time from birth
```

```
        of cluster
135         elif int(fileb[5:-7])>160:
136             t_t.append(int(fileb[5:-7])-140)
137 if len(ms)>0:
138     z = np.zeros(shape=(len(ms),10))
139     z[:,0] = ids
140     z[:,1] = id1
141     z[:,2] = id2
142     z[:,3] = t_t
143     z[:,4] = ms
144     z[:,5] = mb1
145     z[:,6] = mb2
146     z[:,7] = ks
147     z[:,8] = k1
148     z[:,9] = k2
149     np.savetxt(f'triple_{id_imbh}.txt',z)
```

Bibliography

[1] Long Wang et al. "PETAR: a high-performance N-body code for modelling massive collisional stellar systems". In: 497.1 (Sept. 2020), pp. 536–555. DOI: 10.1093/mnras/staa1915. arXiv: 2006.16560 [astro-ph.IM].

[2] Nicola Giacobbo, Michela Mapelli, and Mario Spera. "Merging black hole binaries: the effects of progenitor's metallicity, mass-loss rate and Eddington factor". In: 474.3 (Mar. 2018), pp. 2959–2974. DOI: 10.1093/mnras/stx2933. arXiv: 1711.03556 [astro-ph.SR].

[3] Eva Noyola, Karl Gebhardt, and Marcel Bergmann. "Central Dynamics of Globular Clusters: the Case for a Black Hole in ω Centauri". In: *Dynamical Evolution of Dense Stellar Systems*. Ed. by Enrico Vesperini, Mirek Giersz, and Alison Sills. Vol. 246. May 2008, pp. 341–345. DOI: 10.1017/S1743921308015895.

[4] N. Lützgendorf et al. "Kinematic signature of an intermediate-mass black hole in the globular cluster NGC 6388". In: 533, A36 (Sept. 2011), A36. DOI: 10.1051/0004-6361/201116618. arXiv: 1107.4243 [astro-ph.GA].

[5] Roeland P. van der Marel and Jay Anderson. "New Limits on an Intermediate-Mass Black Hole in Omega Centauri. II. Dynamical Models". In: 710.2 (Feb. 2010), pp. 1063–1088. DOI: 10.1088/0004-637X/710/2/1063. arXiv: 0905.0638 [astro-ph.GA].

[6] B. P. Abbott, LIGO Scientific Collaboration, and Virgo Collaboration. "Binary Black Hole Population Properties Inferred from the First and Second Observing Runs of Advanced LIGO and Advanced Virgo". In: 882.2, L24 (Sept. 2019), p. L24. DOI: 10.3847/2041-8213/ab3800. arXiv: 1811.12940 [astro-ph.HE].

[7] Jonathan R. Gair et al. "Exploring intermediate and massive black-hole binaries with the Einstein Telescope". In: *General Relativity and Gravitation* 43.2 (Oct. 2010), pp. 485–518. DOI: 10.1007/s10714-010-1104-3. URL: https://doi.org/10.1007%2Fs10714-010-1104-3.

[8] Michela Mapelli. "Massive black hole binaries from runaway collisions: the impact of metallicity". In: 459.4 (July 2016), pp. 3432–3446. DOI: 10.1093/mnras/stw869. arXiv: 1604.03559 [astro-ph.GA].

[9] Francesco Paolo Rizzuto et al. "Intermediate mass black hole formation in compact young massive star clusters". In: 501.4 (Mar. 2021), pp. 5257–5273. DOI: 10.1093/mnras/staa3634. arXiv: 2008.09571 [astro-ph.GA].

[10] Carl L. Rodriguez et al. "Modeling Dense Star Clusters in the Milky Way and beyond with the Cluster Monte Carlo Code". In: 258.2, 22 (Feb. 2022), p. 22. DOI: 10.3847/1538-4365/ac2edf. arXiv: 2106.02643 [astro-ph.GA].

[11] Mirek Giersz et al. "MOCCA code for star cluster simulations - II. Comparison with N-body simulations". In: 431.3 (May 2013), pp. 2184–2199. DOI: 10.1093/mnras/stt307. arXiv: 1112.6246 [astro-ph.GA].

[12] R. Abbott, LIGO Scientific Collaboration, and Virgo Collaboration. "GW190521: A Binary Black Hole Merger with a Total Mass of 150 $M_{\odot}$". In: 125.10, 101102 (Sept. 2020), p. 101102. DOI: 10.1103/PhysRevLett.125.101102. arXiv: 2009.01075 [gr-qc].

[13] Charles J. Lada and Elizabeth A. Lada. "Embedded Clusters in Molecular Clouds". In: 41 (Jan. 2003), pp. 57–115. DOI: 10.1146/annurev.astro.41.011802.094844. arXiv: astro-ph/0301540 [astro-ph].

[14] James Binney and Scott Tremaine. *Galactic Dynamics: Second Edition*. 2008.

[15] Simon F. Portegies Zwart, Stephen L. W. McMillan, and Mark Gieles. "Young Massive Star Clusters". In: 48 (Sept. 2010), pp. 431–493. DOI: 10.1146/annurev-astro-081309-130834. arXiv: 1002.1961 [astro-ph.GA].

[16] Anil Seth et al. "Nuclear Star Clusters & Black Holes". In: *Hunting for the Dark: the Hidden Side of Galaxy Formation*. Ed. by Victor P. Debattista and C. C. Popescu. Vol. 1240. American Institute of Physics Conference Series. June 2010, pp. 227–230. DOI: 10.1063/1.3458493. arXiv: 1002.0824 [astro-ph.CO].

[17] Ivan King. "The structure of star clusters. I. an empirical density law". In: 67 (Oct. 1962), p. 471. DOI: 10.1086/108756.

[18] Ivan R. King. "The structure of star clusters. III. Some simple dynamical models". In: 71 (Feb. 1966), p. 64. DOI: 10.1086/109857.

[19] Edwin E. Salpeter. "The Luminosity Function and Stellar Evolution." In: 121 (Jan. 1955), p. 161. DOI: 10.1086/145971.

[20] Pavel Kroupa. "On the variation of the initial mass function". In: 322.2 (Apr. 2001), pp. 231–246. DOI: 10.1046/j.1365-8711.2001.04022.x. arXiv: astro-ph/0009005 [astro-ph].

[21] James Binney and Scott Tremaine. *Galactic dynamics*. 1987.

[22] Lyman Spitzer. *Dynamical evolution of globular clusters*. 1987.

[23] Simon F. Portegies Zwart and Stephen L. W. McMillan. "The Runaway Growth of Intermediate-Mass Black Holes in Dense Star Clusters". In: 576.2 (Sept. 2002), pp. 899–907. DOI: 10.1086/341798. arXiv: astro-ph/0201055 [astro-ph].

[24] D. C. Heggie. "Binary evolution in stellar dynamics." In: 173 (Dec. 1975), pp. 729–787. DOI: 10.1093/mnras/173.3.729.

[25] Sara Rastello et al. "Dynamics of binary black holes in low-mass young star clusters". In: 507.3 (Nov. 2021), pp. 3612–3625. DOI: 10.1093/mnras/stab2355. arXiv: 2105.01669 [astro-ph.GA].

[26] Michela Mapelli. "Binary black hole mergers: formation and populations". In: *Frontiers in Astronomy and Space Sciences* 7, 38 (July 2020), p. 38. DOI: 10.3389/fspas.2020.00038. arXiv: 2105.12455 [astro-ph.HE].

[27] Ugo N. Di Carlo et al. "Merging black holes in young star clusters". In: 487.2 (Aug. 2019), pp. 2947–2960. DOI: 10.1093/mnras/stz1453. arXiv: 1901.00863 [astro-ph.HE].

[28] Michela Mapelli et al. "Mass and Rate of Hierarchical Black Hole Mergers in Young, Globular and Nuclear Star Clusters". In: *Symmetry* 13.9 (Sept. 2021), p. 1678. DOI: 10.3390/sym13091678. arXiv: 2007.15022 [astro-ph.HE].

[29] Marc Favata, Scott A. Hughes, and Daniel E. Holz. "How Black Holes Get Their Kicks: Gravitational Radiation Recoil Revisited". In: 607.1 (May 2004), pp. L5–L8. DOI: 10.1086/421552. arXiv: astro-ph/0402056 [astro-ph].

[30] Manuela Campanelli et al. "Large Merger Recoils and Spin Flips from Generic Black Hole Binaries". In: 659.1 (Apr. 2007), pp. L5–L8. DOI: 10.1086/516712. arXiv: gr-qc/0701164 [gr-qc].

[31] Carlos O. Lousto and Yosef Zlochower. "Hangup Kicks: Still Larger Recoils by Partial Spin-Orbit Alignment of Black-Hole Binaries". In: 107.23, 231102 (Dec. 2011), p. 231102. DOI: 10.1103/PhysRevLett.107.231102. arXiv: 1108.2009 [gr-qc].

[32] Carl L. Rodriguez et al. "Black holes: The next generation—repeated mergers in dense star clusters and their gravitational-wave properties". In: 100.4, 043027 (Aug. 2019), p. 043027. DOI: 10.1103/PhysRevD.100.043027. arXiv: 1906.10260 [astro-ph.HE].

[33] S. E. Woosley and Alexander Heger. "The Pair-instability Mass Gap for Black Holes". In: *The Astrophysical Journal Letters* 912.2 (May 2021), p. L31. DOI: 10.3847/2041-8213/abf2c4. URL: https://doi.org/10.3847%2F2041-8213%2Fabf2c4.

[34] Mirek Giersz et al. "MOCCA code for star cluster simulations - IV. A new scenario for intermediate mass black hole formation in globular clusters". In: 454.3 (Dec. 2015), pp. 3150–3165. DOI: 10.1093/mnras/stv2162. arXiv: 1506.05234 [astro-ph.GA].

[35] P. Kustaanheimo et al. In: 1965.218 (1965), pp. 204–219. DOI: doi:10.1515/crll.1965.218.204. URL: https://doi.org/10.1515/crll.1965.218.204.

[36] Seppo Mikkola and Sverre J. Aarseth. "An Implementation of N-Body Chain Regularization". In: *Celestial Mechanics and Dynamical Astronomy* 57.3 (Nov. 1993), pp. 439–459. DOI: 10.1007/BF00695714.

[37] Tomoyoshi Ito et al. "A special-purpose N-body machine GRAPE-1". In: *Computer Physics Communications* 60.2 (Sept. 1990), pp. 187–194. DOI: 10.1016/0010-4655(90)90003-J.

[38] Simon F. Portegies Zwart, Robert G. Belleman, and Peter M. Geldof. "High-performance direct gravitational N-body simulations on graphics processing units". In: 12.8 (Nov. 2007), pp. 641–650. DOI: 10.1016/j.newast.2007.05.004. arXiv: astro-ph/0702058 [astro-ph].

[39] Sverre J. Aarseth. *Gravitational N-Body Simulations*. 2003.

[40] R. Capuzzo-Dolcetta, M. Spera, and D. Punzo. "A fully parallel, high precision, N-body code running on hybrid computing platforms". In: *Journal of Computational Physics* 236 (Mar. 2013), pp. 580–593. DOI: 10.1016/j.jcp.2012.11.013. arXiv: 1207.2367 [astro-ph.IM].

[41] Sverre J. Aarseth. "From NBODY1 to NBODY6: The Growth of an Industry". In: 111.765 (Nov. 1999), pp. 1333–1346. DOI: 10.1086/316455.

[42] Long Wang et al. "NBODY6++GPU: ready for the gravitational million-body problem". In: 450.4 (July 2015), pp. 4070–4080. DOI: 10.1093/mnras/stv817. arXiv: 1504.03687 [astro-ph.IM].

[43] R. Spurzem. "Direct N-body Simulations". In: *Journal of Computational and Applied Mathematics* 109 (Sept. 1999), pp. 407–432. arXiv: astro-ph/9906154 [astro-ph].

[44] M. Hénon. "Monte Carlo Models of Star Clusters (Part of the Proceedings of the IAU Colloquium No. 10, held in Cambridge, England, August 12-15, 1970.)" In: 13.2 (Oct. 1971), pp. 284–299. DOI: 10.1007/BF00649159.

[45] J. M. Fregeau et al. "Stellar collisions during binary-binary and binary-single star interactions". In: 352.1 (July 2004), pp. 1–19. DOI: 10.1111/j.1365-2966.2004.07914.x. arXiv: astro-ph/0401004 [astro-ph].

[46] Jarrod R. Hurley, Christopher A. Tout, and Onno R. Pols. "Evolution of binary stars and the effect of tides on binary populations". In: 329.4 (Feb. 2002), pp. 897–928. DOI: 10.1046/j.1365-8711.2002.05038.x. arXiv: astro-ph/0201220 [astro-ph].

[47] Mitchell C. Begelman, Marta Volonteri, and Martin J. Rees. "Formation of supermassive black holes by direct collapse in pre-galactic haloes". In: 370.1 (July 2006), pp. 289–298. DOI: 10.1111/j.1365-2966.2006.10467.x. arXiv: astro-ph/0602363 [astro-ph].

[48] Piero Madau and Martin J. Rees. "Massive Black Holes as Population III Remnants". In: 551.1 (Apr. 2001), pp. L27–L30. DOI: 10.1086/319848. arXiv: astro-ph/0101223 [astro-ph].

[49] Mitchell C. Begelman and Martin J. Rees. "The fate of dense stellar systems". In: 185 (Dec. 1978), pp. 847–860. DOI: 10.1093/mnras/185.4.847.

[50] S. F. Portegies Zwart et al. "Star cluster ecology. III. Runaway collisions in young compact star clusters". In: 348 (Aug. 1999), pp. 117–126. arXiv: astro-ph/9812006 [astro-ph].

[51] Simon F. Portegies Zwart et al. "Formation of massive black holes through runaway collisions in dense young star clusters". In: 428.6984 (Apr. 2004), pp. 724–726. DOI: 10.1038/nature02448. arXiv: astro-ph/0402622 [astro-ph].

[52] M. Coleman Miller and Douglas P. Hamilton. "Production of Intermediate-Mass Black Holes in Globular Clusters". In: *Two Years of Science with Chandra*. Ed. by Aneta Siemiginowska. Sept. 2001, 87, p. 87.

[53] Edward J. M. Colbert and Richard F. Mushotzky. "The Nature of Accreting Black Holes in Nearby Galaxy Nuclei". In: 519.1 (July 1999), pp. 89–107. DOI: 10.1086/307356. arXiv: astro-ph/9901023 [astro-ph].

[54] Andreas H. W. Küpper et al. "Mass segregation and fractal substructure in young massive clusters - I. The McLuster code and method calibration". In: 417.3 (Nov. 2011), pp. 2300–2317. DOI: 10.1111/j.1365-2966.2011.19412.x. arXiv: 1107.2395 [astro-ph.GA].

[55] T. Fukushige and D. C. Heggie. "The time-scale of escape from star clusters". In: 318.3 (Nov. 2000), pp. 753–761. DOI: 10.1046/j.1365-8711.2000.03811.x. arXiv: astro-ph/9910468 [astro-ph].

[56] H. Sana et al. "Binary Interaction Dominates the Evolution of Massive Stars". In: *Science* 337.6093 (July 2012), p. 444. DOI: 10.1126/science.1223344. arXiv: 1207.6397 [astro-ph.SR].

[57] Maxwell Moe and Rosanne Di Stefano. "Mind Your Ps and Qs: The Interrelation between Period (P) and Mass-ratio (Q) Distributions of Binary Stars". In: 230.2, 15 (June 2017), p. 15. DOI: 10.3847/1538-4365/aa6fb6. arXiv: 1606.05347 [astro-ph.SR].

[58] Stefano Torniamenti et al. "The impact of binaries on the evolution of star clusters from turbulent molecular clouds". In: 507.2 (Oct. 2021), pp. 2253–2266. DOI: 10.1093/mnras/stab2238. arXiv: 2104.12781 [astro-ph.GA].

[59] Josh Barnes and Piet Hut. "A hierarchical O(N log N) force-calculation algorithm". In: 324.6096 (Dec. 1986), pp. 446–449. DOI: 10.1038/324446a0.

[60] Long Wang, Keigo Nitadori, and Junichiro Makino. *SDAR: Slow-Down Algorithmic Regularization code for solving few-body problems*. Astrophysics Source Code Library, record ascl:2002.001. Feb. 2020. ascl: 2002.001.

[61] Masaki Iwasawa et al. *FDPS: Framework for Developing Particle Simulators*. Astrophysics Source Code Library, record ascl:1604.011. Apr. 2016. ascl: 1604.011.

[62] Shoichi Oshino, Yoko Funato, and Junichiro Makino. "Particle-Particle Particle-Tree: A Direct-Tree Hybrid Scheme for Collisional N-Body Simulations". In: 63 (Aug. 2011), p. 881. DOI: 10.1093/pasj/63.4.881. arXiv: 1101.5504 [astro-ph.EP].

[63] Masaki Iwasawa, Simon Portegies Zwart, and Junichiro Makino. "GPU-enabled particle-particle particle-tree scheme for simulating dense stellar cluster system". In: *Computational Astrophysics and Cosmology* 2, 6 (July 2015), p. 6. DOI: 10.1186/s40668-015-0010-1. arXiv: 1506.04553 [astro-ph.IM].

[64] Jarrod R. Hurley, Onno R. Pols, and Christopher A. Tout. "Comprehensive analytic formulae for stellar evolution as a function of mass and metallicity". In: 315.3 (July 2000), pp. 543–569. DOI: 10.1046/j.1365-8711.2000.03426.x. arXiv: astro-ph/0001295 [astro-ph].

[65] Jo Bovy. "galpy: A python Library for Galactic Dynamics". In: 216.2, 29 (Feb. 2015), p. 29. DOI: 10.1088/0067-0049/216/2/29. arXiv: 1412.3451 [astro-ph.GA].

[66] Chris L. Fryer et al. "Compact Remnant Mass Function: Dependence on the Explosion Mechanism and Metallicity". In: 749.1, 91 (Apr. 2012), p. 91. DOI: 10.1088/0004-637X/749/1/91. arXiv: 1110.1726 [astro-ph.SR].

[67] Nicola Giacobbo and Michela Mapelli. "Revising Natal Kick Prescriptions in Population Synthesis Simulations". In: 891.2, 141 (Mar. 2020), p. 141. DOI: 10.3847/1538-4357/ab7335. arXiv: 1909.06385 [astro-ph.HE].

[68] M. Atakan Gürkan, John M. Fregeau, and Frederic A. Rasio. "Massive Black Hole Binaries from Collisional Runaways". In: 640.1 (Mar. 2006), pp. L39–L42. DOI: 10.1086/503295. arXiv: astro-ph/0512642 [astro-ph].

[69] S. Rastello et al. "Stellar black hole binary mergers in open clusters". In: 483.1 (Feb. 2019), pp. 1233–1246. DOI: 10.1093/mnras/sty3193. arXiv: 1811.10628 [astro-ph.GA].